# Global acetylome profiling indicates EPA impedes but OA promotes prostate cancer motility through altered acetylation of PFN1 and FLNA

Chao He[1], Xiuyuan Chen[2], Ying Chen[1], Jianying Sun[1], Manting Qi[1], Sonia Rocha[3], Mu Wang[1,2*]

[1]Academy of Pharmacy, Xi'an Jiaotong-Liverpool University, Suzhou, Jiangsu 215123, China

[2] Department of Biological Sciences, Xi'an Jiaotong-Liverpool University, Suzhou, Jiangsu 215123, China

[3] Department of Molecular Physiology and Cell Signalling, Institute of Systems, Molecular and Integrative Biology, University of Liverpool, Liverpool L69 7ZB, United Kingdom

## Corresponding author:

Mu Wang, Ph.D.

Professor, Academy of Pharmacy

Xi'an Jiaotong-Liverpool University

111 Ren'ai Road, Suzhou 215123, China.

Tel: +86 512 8818 4673

E-mail: mu.wang@xjtlu.edu.cn

**Keywords:** ω-3 polyunsaturated fatty acids, Cell migration, Mass spectrometry, Lysine acetylation, Prostate cancer

## Abbreviations

PCa, prostate cancer; PUFAs, polyunsaturated fatty acids; MUFA, monounsaturated fatty acid; OA, oleic acid; EPA, eicosapentaenoic acid; PFN1, Profilin-1; FLNA, Filamin A; F-actin, filamentous actin; acetyl-CoA, acetyl Coenzyme A; DTT, dithiothreitol; TFA, trifluoroacetic acid; IAP, immunoaffinity purification; FA, formic acid; DDA, data-dependent analysis; LFQ, label-free quantitation; FDR, false discovery rate; GO, Gene Ontology; IP, immunoprecipitation; PD, Proteome Discoverer; BP, biological process; CC, cellular component; MF, molecular function; ABD, actin-binding domain;

**Word count**: 8261

## Abstract

Prostate cancer (PCa) is one of the leading causes of cancer morbidity and mortality in men. Metastasis is the main cause of PCa-associated death. Recent evidence indicated a significant reduction in PCa mortality associated with higher ω-3 polyunsaturated fatty acids (PUFAs) consumption. However, the underlying mechanisms remained elusive. In this study, we applied global acetylome profiling to study the effect of fatty acids treatment. Results indicated that oleic acid (OA, monounsaturated fatty acid, MUFA, 100 μM) elevates while EPA (eicosapentaenoic acid, 100 μM) reduces the acetyl-CoA level, which alters the global acetylome. After treatment, two crucial cell motility regulators, PFN1 and FLNA, were found with altered acetylation levels. OA increased the acetylation of PFN1 and FLNA, whereas EPA decreased PFN1 acetylation level. Furthermore, OA promotes while EPA inhibits PCa migration and invasion. Immunofluorescence assay indicated that EPA impedes the formation of lamellipodia or filopodia through reduced localization of PFN1 and FLNA to the leading edge of cells. Therefore, perturbed acetylome may be one critical step in fatty acid-affected cancer cell motility. This study provides some new insights into the response of ω-3 PUFAs treatment and a better understanding of cancer cell migration and invasion modulation.

## Significance Statement

Prostate cancer is one of the leading causes of cancer morbidity and mortality in men. As progresses to the advanced stage, prostate cancer cells infiltrate through the basal lamina and lymph nodes, subsequently metastasizing to distant organs. Consequently, the 5-year survival rate declines to approximately 31%. Recently, various studies focused on the effect of diet and lifestyle factors, especially ω-3 polyunsaturated fatty acids (ω-3 PUFAs), on prostate cancer risk. This association may result from the active fatty acid metabolic nature of prostate cancer cells. In this study, our results suggested that Oleic Acid (OA, ω-9 monounsaturated fatty acids) or eicosapentaenoic acid (EPA, one of the main components of Fish Oil, ω-3 PUFA) perturb the acetylome in prostate cancer cells. Notably, altered acetylation was observed in PFN1 and FLNA, two pivotal regulators of cell motility. Consequently, these changes influence the migration and invasion abilities of prostate cancer cells through their effects on F-actin organization. Thus, a therapeutic window may exist in treating cancer metastasis by targeting PFN1 and FLNA and their regulators. Also, this study emphasizes the importance of fatty acid uptake in treating prostate cancer metastasis.

## Introduction

Prostate cancer (PCa) is one of the leading causes of cancer morbidity and mortality in men [1]. In China, prostate cancer burden significantly increased recently, particularly in older people [2,3]. In Europe, it is the most common primary site in men and the third cause of death from cancer [4]. It is estimated that in 2024, prostate cancer is expected to emerge as the most prevalent form of cancer and the second leading cause of cancer-related mortality among men in the USA [5]. Although the death rate began to decrease in the early 1990s, the decline tendency ceased in recent years [6]. What is worse is that the incidence of advanced-stage prostate cancer increased rapidly, with the 5-year survival rate dropping to around 31% [5-7]. When progressed to the advanced stage, prostate cancer cells invade through the basal lamina and lymph nodes and then metastasize to distant organs, such as livers, lungs or bones, which is the main cause of prostate cancer-associated death [8]. Therefore, it is urgent to decipher the critical factors of prostate cancer metastasis to improve the prognosis.

Cancer metastasis is a multi-step process mainly based on cell migration and invasion [9]. During migration and invasion, actin filaments undergo reorganization to extend distinct membrane protrusions, for instance, lamellipodia or filopodia. In lamellipodia, actin filaments are assembled into the branching networks; nevertheless, they are organized into long parallel bundles when forming filopodia [9-13]. The assembly and reorganization of actin filaments are tightly regulated during the migration or invasion cycle. On the one hand, the assemble and disassemble process is modulated by many actin monomer binding proteins, including thymosin β4, twinfillin and Arp2/3 complex, particularly Profilin-1 (PFN1) [9], which plays a critical role in actin homeostasis at the leading edge of membrane protrusion [14,15]. On

the other hand, the organization of filamentous actin (F-actin) is regulated by cross-linking and bundling proteins, such as Filamin A (FLNA). It contributes to orthogonal branching or cross-linking of F-actin [9,16]. Considering the crucial role of PFN1 and FLNA in regulating F-actin and orchestrating cell migration and invasion, the detailed study may lead to a better understanding of cancer metastasis.

Recently, various studies focused on the effect of diet and lifestyle factors, especially ω-3 polyunsaturated fatty acids (ω-3 PUFAs), on prostate cancer risk [17-21]. Although the evidence of ω-3 PUFAs intake and prostate cancer incidence is controversial [17,18], several studies indicated a significant reduction of prostate cancer mortality associated with higher ω-3 PUFAs consumption [19-21]. This may result from the active fatty acid metabolic nature of prostate cancer cells [22,23]. Increased fatty acid utilization, particularly fatty acid β-oxidation, provides cells with acetyl-CoA, one central metabolite that regulates many key biological processes through protein acetylation [24]. Here in the present study, we treated prostate cancer cells with Oleic Acid (OA, ω-9 monounsaturated fatty acids) or eicosapentaenoic acid (EPA, one of the main components of Fish Oil, ω-3 PUFA) to investigate how these different fatty acids influence their behavior through the altered acetyl-CoA level and protein acetylation. As a result, those two fatty acids changed the acetylation of PFN1 and FLNA, which subsequently affects prostate cancer cell migration and invasion via F-actin organization. Our study provides new insight into fatty acid metabolism and cell motility of prostate cancer.

## Materials and methods

### Cell lines and reagents

Prostate cancer cell lines PC-3 and LNCaP clone FGC were purchased from Stem Cell Bank, Chinese Academy of Sciences (Shanghai, China). PC-3 cells were cultured in F-12K medium (Hyclone, Logan, UT, USA) with 10% fetal bovine serum (Biological Industries, Kibbutz Beit Haemek, Israel). LNCaP cells were cultured in RPMI-1640 medium with the final concentration of 10% fetal bovine serum (Biological Industries), 2 mM L-Glutamine (Beyotime Biotechnology, Shanghai, China) and 1 mM sodium pyruvate (Sigma-Aldrich, St. Louis, MO, USA). All cells were incubated in a humidified atmosphere with 5% $CO_2$ at 37 °C.

EPA was kindly provided by Yuekang Biotechnology Co., Ltd. (Suzhou, China). EPA and oleic acid (OA, Macklin, Shanghai, China) were dissolved in ethanol (Sinopharm, Shanghai, China) to obtain a stock solution with a concentration of 100 mM. The cells were treated with a final concentration of 100 μM OA or EPA, while the control group received an equal amount of ethanol (0.1%, v/v). Cells were harvested 24 h after treatment for further study. The concentration of EPA at 100 μM was determined to be a sublethal dose [25].

### Cellular Acetyl Coenzyme A quantification

The concentration of cellular Acetyl Coenzyme A (Acetyl-CoA) was determined using a sandwich ELISA-based kit (Sangon, Shanghai, China) following the manufacturer's instructions. Briefly, harvested cells were washed with PBS twice. For each 1 x $10^6$ cells, add 250 μL PBS to keep the cells suspended. After sonication (five bursts for five seconds and cool on ice for five seconds between each burst), cell lysate was centrifuged for 10 min at 1500 x g at 4 °C to remove the cell fragments. For Acetyl-CoA detection, 100 μL of samples or standards were added to reaction

wells and incubated for 90 min at 37 ℃. After washing, the biotin-conjugated antibody was added to each well and incubated for 60 min at 37 °C. The antibody was discarded, and the wells were washed four times, followed by incubating HRP-conjugated streptavidin working solution for 30 min at 37 °C. After four times of wash, substrate reagent was added and developed for 15 min at 37 °C. The stop solution was added to stop the reaction, and the OD value was immediately measured at the wavelength of 450 nm with a microplate reader (SpectraMax i3X, Molecular Devices, CA, USA). The results were normalized by cell number in each group. Three technical replicates were performed for each sample.

**Protein extraction and digestion for proteomics**

PC-3 cells were seeded in the 150 mm culture dish ($1x10^6$ cells per dish) and treated for 24 h. Four batches of cells were harvested and lysed at room temperature using urea lysis buffer containing 9 M urea (Sigma), 20 mM HEPES (Sigma), 1 mM sodium orthovanadate (Sigma), 2.5 mM sodium pyrophosphate (Sigma), 1 mM β-glycerophosphate (Sigma). The lysate was sonicated three times. For each sonication cycle, sonicate for 15 s and cool on ice for 1 min. Then, the lysate was centrifugated at 20000 x g for 15 min at room temperature, after which the supernatant was transferred to a new tube. The protein concentration was determined by the BCA protein quantification kit (Beyotime). After reduction with dithiothreitol (DTT, sigma) and alkylation with iodoacetamide (Aladdin, Shanghai, China), the protein was diluted 4-fold by 20 mM HEPES (pH 8.0) and was digested by trypsin (1:75, Promega, Madison, WI, USA) overnight at 37 °C. Acidify the digest by adding trifluoroacetic acid (TFA, sequencing grade, Thermo Fisher Scientific, Waltham, MA, USA) to the digest at a final concentration of 1%, followed by centrifuge at 2000 x g at room temperature. Transfer the supernatant to a new tube, after which the peptides were

purified by Sep-Pak® C18 Purification column (Waters, Milford, MA, USA) and lyophilized.

**Enrichment of peptide with lysine acetylation**

The peptide enrichment was carried out using PTMScan® Acetyl-Lysine Motif [Ac-K] Kit (Cell Signaling Technology, Danvers, MA, USA) following the instructions from the manufacturer. In brief, lyophilized peptides were resuspended with immunoaffinity purification (IAP) buffer and incubated with pre-cleaned antibody-bead slurry at 4 °C for 2 h. After washing, enriched peptides were eluted with 0.15% TFA, purified using MonoSpin $C_{18}$ column (GL Science, Tokyo, Japan) and lyophilized.

**Label-free based acetylomics**

Enriched peptides (2 μg) were analyzed using EASY-nLC 1000 coupled with LTQ-Orbitrap Elite (Thermo Fisher). The analytical column used was MonoCap™ $C_{18}$ High Resolution 3000 column (5020-MonoCap C18 High Resolution 3000, 0.1 mm, GL Science). Briefly, lyophilized peptides were resuspended with 0.1% formic acid (FA, Fluka, Charlotte, North Carolina, USA) and separated by buffer system: buffer A (0.1% FA) and buffer B (98% acetonitrile, 0.1% FA). The flow rate was 300 nL/min, and the gradient was set as follows: 5% B, 0 min; 5% ~ 50% B, 315 min; 50% ~ 90% B, 35 min; 90% B, 20 min; 90% ~ 5% B, 15 min; 5% B,10 min. For the MS method, the NSI source was used, the spray voltage was 1.8 kV, and the capillary temperature was 275°C. Data-dependent analysis (DDA) was chosen as the data acquisition mode to get a higher-quality secondary spectrum. The resolution of full mass scanning was set at 60,000, the scan range 300 ~ 2000 m/z, and the resolution of tandem scanning was set at 15,000. The normalized collision energy of HCD was 35% x 5 V, activation time was 0.1 ms, and isolation width = 1.0 m/z.

**Data analysis of acetylome profiling**

MaxQuant software (Version 1.6.7.0) was used for label-free quantitation (LFQ) analysis. Variable modifications contained oxidation, acetyl (K), and acetyl (protein N-term); fixed modifications included carbamidomethyl. The false discovery rate (FRD) cut-off value was set to 0.01. The unique peptides with acetylation are screened out. The mass spectrometry proteomics data have been deposited to the ProteomeXchange Consortium with the dataset identifier PXD044068.

For further analysis, R software (Version 4.2.1) was used with packages of limma (Version 3.52.2) for expression analysis and clusterProfiler (Version 4.4.4) for Gene Ontology (GO) enrichment [26,27]. Candidates must meet the following criteria: *P*-value < 0.05, at least in one comparison group among EPA-Ethanol, OA-Ethanol or EPA-OA; and fold change > 1.5 between EPA and OA treated groups.

**Immunoprecipitation (IP)**

Harvested cells were lysed with RIPA lysis buffer (Beyotime), supplied with the cocktail of protease inhibitors, phosphatase inhibitors and deacetylase inhibitors (Beyotime). BCA protein quantification kit (Beyotime) was used to determine protein concentration. Total 750 μg of proteins were used for IP. The proteins were incubated with anti-PFN1 (Abways, Shanghai, China), anti-FLNA (Santa Cruz Biotechnology, Dallas, TX, USA) or mouse/rabbit IgG (Beyotime) antibodies at 4 °C overnight. Afterwards, protein A/G Sepharose beads (Abcam, Cambridge, MA, USA) were used for capturing the antibodies. After 2 h of incubation at 4 °C, the beads were collected by centrifuging the mixture at 2,000 x g for 2 min, followed by three times of wash with PBST. Proteins were eluted with 2 × loading buffer and denatured at 100°C for 10 min.

**In-gel digestion and LC-MS/MS analysis**

Eluted proteins were loaded into polyacrylamide gels. After 10 min of electrophoresis, gels were cut into pieces and destained with 50 mM $NH_4HCO_3$ (Sigma) in 50 % (v/v) acetonitrile (Thermo) until clear. Then, acetonitrile was added for dehydration. Gel pieces were incubated with 10 mM dithiothreitol (DTT, Sigma) for 1 h at 37 °C. After dehydration with acetonitrile, gel pieces were incubated with 55 mM of iodoacetamide (Aladdin) for 45 min at room temperature in the dark, followed by a washing step using 50 mM $NH_4HCO_3$. After dehydration, gel pieces were digested with 10 ng/μL trypsin overnight at 37 °C. Digested peptides were extracted sequentially with 50 % acetonitrile/5 % FA and 100 % acetonitrile, after which the peptides were lyophilized and resuspended in buffer A (2 % acetonitrile, 0.1 % FA)

The peptides were separated with $C_{18}$ column (Double nanoViper™ PepMap™ Neo UHPLC column, DNV75150PN, 0.075 mm, Thermo Fisher) by buffers A and B (80 % acetonitrile, 0.1 % FA). The flow rate was 300 nL/min, and the gradient was set as follows: 5 % B, 0 min; 5 % ~ 8 % B, 5 min; 8 % ~ 32 % B, 40 min; 32 % ~ 99 % B, 9 min. Separated peptides were then analyzed by Q Exactive™ Plus (Thermo). The electrospray voltage was 2.2 kV, and the capillary temperature was 320°C. The m/z scan range was 400 to 1600. More instrument settings are available in Table S1. The MS/MS data were processed with Proteome Discoverer (PD v2.5). Variable modifications contained oxidation, acetyl (K), and acetyl (protein N-term); fixed modifications included carbamidomethyl. Peptide intensities were selected for analysis.

**Western blot analysis**

Harvested cells were lysed with Cell lysis buffer for Western and IP (Beyotime), supplied with the cocktail of protease inhibitors, phosphatase inhibitors and

deacetylase inhibitors (Beyotime). BCA protein quantification kit (Beyotime) was used to determine protein concentration. The equal amounts of proteins were loaded into SurePAGE™ precast gels with a linear gradient between 4 – 20 % (GenScript, Nanjing, China). After separation, proteins were transferred to PVDF membranes (Millipore, Billerica, MA, USA) by eBlot® L1 protein transfer system (GenScript), followed by incubation with QuickBlock™ Blocking Buffer (Beyotime) for 1 h at room temperature. Membranes were then incubated with primary antibodies against β-tubulin (Proteintech, Rosemont, IL, USA), acetyl lysine (PTM-BIO, Hangzhou, Zhejiang, China), PFN1 (Abways) or FLNA (Santa Cruz Biotechnology) overnight at 4 °C. The membranes were then incubated with IRDye® 680 Donkey anti-Rabbit IgG (H + L) or IRDye® 800 Donkey anti-Mouse IgG (H + L) secondary antibodies (LI-COR Corporate, Lincoln, NE, USA) after washing. Protein bands were visualized using Odyssey® DLx Imaging System (LI-COR Corporate) and analyzed using Image Studio Lite (Ver 5.2, LI-COR Corporate). The level of β-tubulin was considered as a loading control. Three biological replicates were conducted for all the immunoblotting assays.

**RNA interference and transfection**

For the downregulation of PFN1 and FLNA, siRNAs (Table S2) were designed and purchased from GenePharma (Suzhou, China). Transient transfection of siRNAs was carried out using an X-Porator H1 electroporation system (Etta Biotech, Suzhou, China) following the instructions from the manufacturer. Briefly, 1-2 x $10^6$ cells were harvested and resuspended in EBEL buffer. After adding the control RNA or siRNAs, the cell suspension was transferred to the cuvette electrode. The electroporation program was set as 150 V of voltage, 1500 μs of duration, 4 of pulse number and 600

ms of interval. Then, transfected cells were washed with culture media and seeded into plates for further analysis.

**RNA isolation and quantitative real-time PCR**

Total RNA was isolated using TRI reagent® (Sigma). The concentrations were determined by Nano-Drop one (Thermo). A total 1 μg of RNA was reverse transcribed into cDNA by the GoScript™ Reverse Transcription System (Promega). For qRT-PCR, GoTaq® qPCR Master Mix (Promega) was used. Quantitative PCR was performed by QuantStudio 5 (Thermo) Real-Time PCR System. The level of TUBB (β-tubulin) was considered as the internal control. The primers for PFN1 are: forward, ATCGTGGGCTACAAGGACTC; reverse, TTGGTGACAGTGACATTGAAGG. For FLNA: forward, GCTCCTGTGGTGTGGCTTA; reverse, AAGAGGCTGGCTGGTTGAC. For TUBB: forward, ATATGTTCCTCGTGCCATCCT; reverse, TCTGCCTCCTTCCGTACCA. Three technical replicates were conducted for each sample.

**Wound-healing assay**

Cells were seeded in six-well plates. A wound was drawn vertically using a 1 mL pipette tip in the six-well plates. Cells were then washed with PBS to remove the detached cells. The fresh medium without FBS was added. Subsequently, the cells were subjected to treatment with ethanol, OA (100 μM), and EPA (100 μM) until the completion of the experiment. Photos were taken at an appropriate time to assess cell migration using a light microscope (ECLIPSE Ti2, Nikon, Tokyo, Japan). All the wound-healing assay had been repeated for three times. Fiji (2.11.0) plug-in “MRI Wound Healing Tool” was applied for the calculation of open wound area.

**Transwell invasion assay**

Cell invasion was assessed by transwell chambers with 8 μm pore polycarbonate membrane (Corning Incorporated, Corning, NY, USA), which were coated with Matrigel (BD Bioscience, Billerica, MA, USA) at 1:7 dilution before use. Treated cells were harvested and adjusted to the same density. For PC-3 cells, 1 x $10^5$ cells were seeded into the upper chamber. For LNCaP cells, 2 x $10^5$ cells were seeded. The lower chambers were filled with culture media that contained 20 % FBS. After 24 h for PC-3 and 48 h for LNCaP, the cells remaining in the upper chambers were scraped off, and the invading cells were stained using the Wright-Giemsa solution (Nanjing Jiancheng Bioengineering Technology, Nanjing, China). For each transwell assay, three images were captured under a microscope (ECLIPSE Ti2), and the numbers of invaded cells were counted.

**Immunofluorescence assay**

The visualization of lamellipodia or filopodia was achieved by staining F-actin with phalloidin. In brief, 5 x $10^4$ cells were seeded per well in 24-well plates and treated for 24 h before immunofluorescence assay. Treated cells were then fixed with 4 % paraformaldehyde (Biosharp, Hefei, China) for 10 min at room temperature, followed by permeation using 0.2% Triton X-100 (Beyotime) for 10 min. After blocking using 5% BSA for 1 h, cells were incubated with primary antibody against PFN1 (Abways) or FLNA (Santa Cruz Biotechnology) at 4 ℃ overnight. After three times of washing, samples were incubated with Actin-Tracker Green-488 (Alexa Fluor 488-conjugated phalloidin, Beyotime) and CoraLite594-conjugated Goat anti-Rabbit or anti-Mouse IgG (H+L) (Proteintech) for 1 h at room temperature. Afterwards, samples were mounted with DAPI containing antifading mounting medium (Beijing Solarbio Science & Technology Co., Ltd., Beijing, China). Images were captured with Confocal Microscope LSM 880 (Zeiss, Oberkochen, Germany).

**Statistical analysis**

The quantitative results are presented as the mean values ± SD. Statistical analysis was carried out using GraphPad Prism 8. One-way or two-way ANOVA with Tukey's or Dunnett's multiple comparison tests were performed when appropriate. Results were considered statistically significant when the $p$-value < 0.05. Statistical significance is demonstrated in the Figures: * $p < 0.05$, ** $p < 0.01$, *** $p < 0.001$.

## Results

### OA or EPA treatment alters cellular acetyl-CoA levels and perturbs global acetylome in prostate cancer cells

To test whether distinct fatty acids alter cellular acetyl-CoA, we determined its level using an ELISA-based kit. PC-3 and LNCaP cells were treated with ethanol (solvent control), OA, and EPA, respectively, for 24 h. Interestingly, compared to the control group, OA treatment increased while EPA reduced cellular acetyl-CoA level (Figure 1A).

Since altered acetyl-CoA level may result in perturbed acetylome, we next applied global acetylome profiling in PC-3 cells, trying to unveil the mechanism of how these fatty acids change the behavior of prostate cancer cells. The workflow is shown in Figure 1B. A total of 538 acetylated peptides were identified in our acetylome profiling. Among all identified peptides, 67 were selected as regulated peptides for the $p$-value < 0.05, at least in one comparison group among EPA-Ethanol, OA-Ethanol or EPA-OA. Finally, 44 peptides representing 41 differentially acetylated proteins were selected as candidates for the fold change was higher than 1.5 between EPA and OA treated groups (Figure 1C). All candidates and the acetylation sites were shown in the volcano plot (Figure 1D). Intriguingly, the acetylation levels of most candidates in the OA group were found to be elevated compared with other groups. Only several proteins showed altered acetylation between EPA and ethanol groups.

We next carried out Gene Ontology (GO) analysis (Table S3). Results suggested many proteins are involved in the biological process (BP) of peroxisome localization, organization or transportation. Also, many candidates were located in the cellular component (CC) of the peroxisomal matrix. This is consistent with the fact that peroxisome is the key organelle responsible for long-chain fatty acid beta-oxidation,

which generates acetyl-CoA. Moreover, some candidates locate in focal adhesion and have the molecular function (MF) of cadherin binding. Since this study mainly focuses on prostate cancer motility and metastasis, Profilin-1 (PFN1) and Filamin A (FLNA) were selected for further investigation due to their critical role in maintaining dynamic homeostasis and meticulous organization of F-actin [9,14-16,28-31].

**Validation of PFN1 and FLNA acetylation**

Since our acetylome results indicated that altered acetylation occurred at K126 of PFN1 and K2569 of FLNA after treatment (Figure 2A & 2B), we next carried out an immunoprecipitation assay for validation. Both proteins were precipitated and examined by the Lysine-acetylation motif antibody. Results showed that, in PC-3 cells, the protein level of both PFN1 and FLNA remained unchanged when treated with OA or EPA. The acetylation of PFN1 was higher in OA treated group and much less in the EPA group, compared with the control group (Figure 2C). Intriguingly, FLNA also showed over acetylation in OA treated group but was similarly acetylated between ethanol and EPA groups (Figure 2D). Since it is possible that FLNA may be acetylated at multiple sites, we further validated its acetylation using mass spectrometry after IP. Results showed that besides K2569, FLNA was acetylated at multiple sites, including K691, K891, K1801 and K2623. Moreover, acetylation patterns were distinct in different groups (Figure S1).

To confirm whether the fatty acid treatment also affects the acetylation of PFN1 and FLNA in LNCaP cells, we investigated their acetylation using a similar approach. Results indicated that PFN1 acetylation was elevated in the OA group while less acetylated in EPA treated group (Figure S2). Unexpectedly, we failed to observe the acetylated band of FLNA in LNCaP cells by Western blot. We then examined the acetylation by using mass spectrometry after IP. As shown in Figure S3, the

acetylation of FLNA only occurred in the OA group at K33 and K691. (Figure S4, S5 and S6 show the uncropped western blot images)

In conclusion, in both PC-3 and LNCaP cells, the acetylation of PFN1 elevated when treated with OA while decreased when treated with EPA. Nevertheless, FLNA acetylation was increased in the wake of OA treatment. Moreover, the acetylation pattern of FLNA changed after treatment with different fatty acids.

**PFN1 and FLNA are key modulators of prostate cancer migration and invasion**

Having validated the acetylation change of PFN1 and FLNA, we next evaluated their function in cancer cell motility through downregulation. Two siRNAs were designed and transfected into PC-3 and LNCaP cells for each gene. The knockdown efficiency was confirmed by qPCR and Western blot 48 hours post-electroporation. As shown in Figure 3A & 3C, both PFN1 and FLNA were successfully knocked down at the mRNA level. Their knockdown was further confirmed by Western blot at the protein level (Figure 3B & 3D, Figure S7). We then evaluated their essentiality in cell motility by wound healing and invasion assay. After electroporation, cells were seeded in 6-well plates and incubated for 48 h before the wound was drawn. Results indicated that PFN1 or FLNA downregulation impeded the migration of PC-3 and LNCaP cells and that the wound narrowed more slowly in downregulated groups than in the control groups (Figure 3E). Similarly, PFN1 or FLNA downregulation compromised the capability of prostate cancer cells to penetrate through the Matrigel-coated transwell chamber (Figure 3F). In the control group, around 75 of PC-3 and 125 of LNCaP cells can be seen in each field. However, it was less than 20 of PC-3 and 45 of LNCaP cells per field in the downregulated groups.

In conclusion, PFN1 and FLNA are vital to prostate cancer migration and invasion.

**OA stimulates while EPA impedes the migration and invasion of prostate cancer cells**

Since PFN1 and FLNA are critical to cancer cell motility, we thus postulated that different fatty acids might affect the migration and invasion through altered acetylation of those two proteins. Therefore, we applied wound-healing assay and transwell invasion assay for functional validation. As expected, when treated with OA, PC-3 cells exhibited higher migration capacity that the wound almost healed after 48 h; while the gap in EPA treated group recovered more slowly, the wound area diminished to about 50% (Figure 4A). Although LNCaP cells migrated more slowly than PC-3 cells, similar results were observed. The wound area narrowed more rapidly in OA treated group than in other groups. After 96 h, the open wound area reduced to less than 70% in the OA group, while it was more than 80% in the EPA group compared with the initial area. These results suggested that OA stimulated while EPA impeded the migration of prostate cancer cells.

Next, we applied an invasion assay by coating the upper chamber of the transwell with Matrigel. Cells were pre-treated for 24 h before harvesting. After incubation of 24 h for PC-3 cells and 48 h for LNCaP cells, the chambers were stained to visualize the invaded cells. As a result, more cells penetrated through the chamber in OA treated group while only few cells did in EPA treated group than the control group, indicating that OA accelerated but EPA decelerated the invasion of prostate cancer cells.

Moreover, we tested whether OA treatment could recover the motility in PFN1 or FLNA downregulated prostate cancer cells. Results suggested that OA partially restored the motility when PFN1 or FLNA were knocked down, compared to the OA

treated control group (Figure S8). These findings indicate that both PFN1 and FLNA are crucial factors in OA stimulated prostate cancer motility.

**Changed cell motility after OA or EPA treatment results from altered F-actin skeleton organization**

Actin remodeling and organization play a critical role in cancer cell migration and invasion. As observed in this study, both PFN1 and FLNA are key modulators of this process. Therefore, the changed acetylation status of those two proteins may affect actin organization. To study whether OA or EPA treatment alters actin skeleton organization, we carried out an immunofluorescence assay. In PC-3 cells, PFN1 located in lamellipodia in the control and OA-treated groups to promote filamentous actin (F-actin) assembly (Figure 5A). Simultaneously, FLNA co-localized with F-actin at lamellipodia, contributing to actin organization in the control and OA-treated groups (Figure 5B). However, only 25% of PC-3 cells in the EPA-treated group exhibited PFN1 or FLNA co-localization with F-actin at lamellipodia. In comparison, it was around 40% in the control group and 60% in the OA-treated group (Figure 5A & 5B, Figure S9 & S10). Interestingly, LNCaP cells tend to form filopodia rather than lamellipodia. As shown in Figure 5C & 5D, filopodia in the control and OA-treated groups filled with bundles of F-actin and more PFN1 and FLNA co-localization. On the contrary, only 10% of PFN1 and 20% of FLNA co-exist with F-actin at filopodia when treated by EPA (Figure 5C & 5D, Figure S11 & S12).

In conclusion, OA or EPA treatment affected F-actin organization through the changed behaviour of PFN1 and FLNA.

## Discussion

Recently, mounting evidence indicated that ω-3 long chain PUFAs, such as DHA or EPA, exhibited a protective effect on prostate cancer [19-21]. However, the mechanisms remained unclear. Herein, our study provides novel evidence that EPA impedes the migration and invasion of prostate cancer. Results suggested that EPA treatment reduced cellular acetyl-CoA level and then altered acetylation of PFN1 and FLNA, two critical factors of actin organization during the formation of lamellipodia or filopodia. Consequently, the migration and invasion of prostate cancer cells were inhibited due to the malfunction of lamellipodia or filopodia. On the contrary, OA (ω-9 monounsaturated fatty acid) elevates the acetyl-CoA level, resulting in over-acetylation of PFN1 and FLNA and accelerating cell migration and invasion.

One pivotal fatty acid metabolism pathway of cancer cells is β-oxidation, especially in prostate cancer [22,23]. It supports the proliferation and metastatic progression of cancer cells with the supplement of ATP, NADPH and, most importantly, acetyl-CoA [32]. Ample evidence suggests that acetyl-CoA is a critical metabolite linking many catabolic and anabolic metabolism and acts as a second messenger regulating many key processes via altered acetylome [24,33]. Moreover, the supplement of Acetyl-CoA enhanced the migration of PC-3 cells while etomoxir, the β-oxidation inhibitor, impeded OA induced migration (Figure S13). Intriguingly, in this study, OA treatment significantly elevated acetyl-CoA concentration; however, when treated with EPA, the acetyl-CoA level was reduced. This may be due to different metabolism pathways based on the unsaturation degrees. Firstly, the oxidation of EPA is more complicated than OA. Polyunsaturated EPA requires the auxiliary enzyme system [34], which decreases the efficiency of β-oxidation. Secondly, another study in our group suggested that prostate cancer cells may harbour distinct preferences in the

utilization of fatty acids with different degrees of unsaturation (data not shown). Further study will be carried out to investigate the influences of these fatty acids on the cellular lipid pool.

Prior studies that have noted the importance of fatty acids supplement and cancer motility, primarily by modulating PPARγ activity, cellular lipid metabolism or epithelial–mesenchymal transition [35-38]. In this study, our novel findings suggest that the acetylation of PFN1 and FLNA, rather than changes in their expression levels, plays a pivotal role in modulating cell motility upon treatment with fatty acids. They are both critical in prostate cancer migration and invasion (Figure 3). On the one hand, PFN1 promotes actin polymerization to support cell migration and invasion [14,15,39]. PFN1 consists of five α-helixes and seven β-sheets. Herein, PFN1 was found acetylated at K126 within helix 5, a critical domain responsible for interacting with actin [40]. Our results suggested that acetylation at K126 may contribute to the binding of PFN1 to actin. That may be the reason why PFN1 was absent at the leading edge of lamellipodia or filopodia upon EPA treatment (Figure 5A & 5C, Figure S9 & S11). Intriguingly, the migration decreased when deacetylation mimic mutation of PFN1 (K126R) was transfected in PC-3 cells (Figure S14). On the other hand, FLNA contributes to orthogonal branching or cross-linking of F-actin [9,16]. As shown in Figure S1A, FLNA consists of one actin-binding domain (ABD) at the N-terminal, 24 Filamin repeats and two hinges. The ABD and Filamin repeat 1-15 form a linear structure termed rod-1 [41-43]. We found that FLNA is acetylated at K691 and K891 in PC-3 cells or K33 and K691 in LNCaP cells within rod-1. Altered acetylation within rod-1 may affect its binding to F-actin and change the tension of the F-actin network [44]. Besides, altered acetylation at K2569 in Filamin repeat 24 may affect the dimerization of FLNA [41]. Although FLNA is acetylated at multiple sites, the overall

acetylation level elevated after OA treatment (Figure 2D). Functionally, more over-acetylated FLNA was found to localize to lamellipodia or filopodia, subserving their formation and prostate cancer cell migration and invasion (Figure 5B & 5D, Figure S10 & S12).

Although we have identified the acetylation sites of PFN1 and FLNA, many questions remain elusive. First, the connection between acetylation and their function is not clear. Second, how their acetylation is regulated needs to be studied. Third, whether acetylation communicates with other types of post-translational modification (for instance, phosphorylation or succinylation) remains to be clarified. Last, besides actin, their interaction partners are also critical and need to be identified. Therefore, further scrutiny will be devoted to deciphering those missing puzzles.

Recently, the role of PFN1 [14,28,45-50] and FLNA [29-31,41,51,52] in cancer has been brought into the limelight. However, few studies focused on the correlation between their acetylation and cancer dissemination. In this study, we found that different fatty acids alter the cellular acetyl-CoA level to perturb the acetylome in prostate cancer; OA contributes to migration and invasion through over-acetylation of PFN1 and FLNA, whereas EPA impedes migration and invasion via reduced acetylation of PFN1 or altered acetylation pattern of FLNA. This is one critical step in fatty acid-affected cancer cell motility. Thus, a therapeutic window may exist in treating cancer metastasis by targeting PFN1 and FLNA and their regulators. Also, this study emphasizes the importance of fatty acid uptake in treating prostate cancer metastasis.

## Supporting information

This article includes supporting information.

## Data availability

The mass spectrometry proteomics data have been deposited to the ProteomeXchange Consortium with the dataset identifier PXD044068. Additional data used and/or analyzed during the current study are available from the corresponding author on reasonable request.

## Acknowledgements

We gratefully acknowledge Professor Sung Kay Chiu and Dr. Sancy Joyson for the technical assistance. The Graphical Abstract and Figure 1B were created with BioRender.com. This work was supported in part by XJTLU Key Program Special Fund–KSF Exploratory Research KSF-E-14 (Mu Wang).

## Conflict of Interest

The authors declare that they have no competing interests.

## Author contributions

Chao He: Conceptualization, Investigation and Writing - original draft; Xiuyuan Chen: Methodology and software; Ying Chen, Jianying Sun and Manting Qi: Methodology, software and Resources; Sonia Rocha and Mu Wang: Project administration, Supervision and Writing - review & editing.

# References


[1] De Silva, F., & Alcorn, J. (2022). A Tale of Two Cancers: A Current Concise Overview of Breast and Prostate Cancer. *Cancers (Basel), 14*(12), 2954-2981. doi: 10.3390/cancers14122954

[2] Xia, C., Dong, X., Li, H., Cao, M., Sun, D., He, S., . . . Chen, W. (2022). Cancer statistics in China and United States, 2022: profiles, trends, and determinants. *Chin Med J (Engl), 135*(5), 584-590. doi: 10.1097/CM9.0000000000002108

[3] Ju, W., Zheng, R., Zhang, S., Zeng, H., Sun, K., Wang, S., . . . He, J. (2023). Cancer statistics in Chinese older people, 2022: current burden, time trends, and comparisons with the US, Japan, and the Republic of Korea. *Sci China Life Sci, 66*(5), 1079-1091. doi: 10.1007/s11427-022-2218-x

[4] Ferlay, J., Colombet, M., Soerjomataram, I., Dyba, T., Randi, G., Bettio, M., . . . Bray, F. (2018). Cancer incidence and mortality patterns in Europe: Estimates for 40 countries and 25 major cancers in 2018. *Eur J Cancer, 103*, 356-387. doi: 10.1016/j.ejca.2018.07.005

[5] Siegel, R. L., Giaquinto, A. N., & Jemal, A. (2024). Cancer statistics, 2024. *CA Cancer J Clin, 74*(1), 12-49. doi: 10.3322/caac.21820

[6] Schafer, E. J., Jemal, A., Wiese, D., Sung, H., Kratzer, T. B., Islami, F., . . . Knudsen, K. E. (2023). Disparities and Trends in Genitourinary Cancer Incidence and Mortality in the USA. *Eur Urol, 84*(1), 117-126. doi: 10.1016/j.eururo.2022.11.023

[7] Miller, K. D., Nogueira, L., Devasia, T., Mariotto, A. B., Yabroff, K. R., Jemal, A., . . . Siegel, R. L. (2022). Cancer treatment and survivorship statistics, 2022. *CA Cancer J Clin, 72*(5), 409-436. doi: 10.3322/caac.21731

[8] Wang, G., Zhao, D., Spring, D. J., & DePinho, R. A. (2018). Genetics and biology of prostate cancer. *Genes Dev, 32*(17-18), 1105-1140. doi: 10.1101/gad.315739.118

[9] Aseervatham, J. (2020). Cytoskeletal Remodeling in Cancer. *Biology (Basel), 9*(11), 385-424. doi: 10.3390/biology9110385

[10] Schaks, M., Giannone, G., & Rottner, K. (2019). Actin dynamics in cell migration. *Essays Biochem, 63*(5), 483-495. doi: 10.1042/EBC20190015

[11] Ridley, A. J., Schwartz, M. A., Burridge, K., Firtel, R. A., Ginsberg, M. H., Borisy, G., . . . Horwitz, A. R. (2003). Cell migration: integrating signals from front to back. *Science, 302*(5651), 1704-1709. doi: 10.1126/science.1092053

[12] Alexandrova, A. Y., Chikina, A. S., & Svitkina, T. M. (2020). Actin cytoskeleton in mesenchymal-to-amoeboid transition of cancer cells. *Int Rev Cell Mol Biol, 356*, 197-256. doi: 10.1016/bs.ircmb.2020.06.002

[13] Izdebska, M., Zielinska, W., Grzanka, D., & Gagat, M. (2018). The Role of Actin Dynamics and Actin-Binding Proteins Expression in Epithelial-to-Mesenchymal Transition and Its Association with Cancer Progression and Evaluation of Possible Therapeutic Targets. *Biomed Res Int, 2018*, 4578373-4578385. doi: 10.1155/2018/4578373

[14] Allen, A., Gau, D., Francoeur, P., Sturm, J., Wang, Y., Martin, R., . . . Roy, P. (2020). Actin-binding protein profilin1 promotes aggressiveness of clear-cell renal cell carcinoma cells. *J Biol Chem, 295*(46), 15636-15649. doi: 10.1074/jbc.RA120.013963

[15] Rotty, J. D., Wu, C., Haynes, E. M., Suarez, C., Winkelman, J. D., Johnson, H. E., . . . Bear, J. E. (2015). Profilin-1 serves as a gatekeeper for actin assembly by Arp2/3-dependent and -independent pathways. *Dev Cell, 32*(1), 54-67. doi: 10.1016/j.devcel.2014.10.026

[16] Chiang, T. S., Wu, H. F., & Lee, F. S. (2017). ADP-ribosylation factor-like 4C binding to filamin-A modulates filopodium formation and cell migration. *Mol Biol Cell, 28*(22), 3013-3028. doi: 10.1091/mbc.E17-01-0059

[17] Wilson, K. M., & Mucci, L. A. (2019). Diet and Lifestyle in Prostate Cancer. *Adv Exp Med Biol, 1210*, 1-27. doi: 10.1007/978-3-030-32656-2_1

[18] Lee, K. H., Seong, H. J., Kim, G., Jeong, G. H., Kim, J. Y., Park, H., . . . Gamerith, G. (2020). Consumption of Fish and omega-3 Fatty Acids and Cancer Risk: An Umbrella Review of

Meta-Analyses of Observational Studies. *Adv Nutr, 11*(5), 1134-1149. doi: 10.1093/advances/nmaa055

[19] Aucoin, M., Cooley, K., Knee, C., Fritz, H., Balneaves, L. G., Breau, R., . . . Seely, D. (2017). Fish-Derived Omega-3 Fatty Acids and Prostate Cancer: A Systematic Review. *Integrative cancer therapies, 16*(1), 32-62. doi: 10.1177/1534735416656052

[20] Szymanski, K. M., Wheeler, D. C., & Mucci, L. A. (2010). Fish consumption and prostate cancer risk: a review and meta-analysis. *Am J Clin Nutr, 92*(5), 1223-1233. doi: 10.3945/ajcn.2010.29530

[21] Bischoff-Ferrari, H. A., Willett, W. C., Manson, J. E., Dawson-Hughes, B., Manz, M. G., Theiler, R., . . . Gaengler, S. (2022). Combined Vitamin D, Omega-3 Fatty Acids, and a Simple Home Exercise Program May Reduce Cancer Risk Among Active Adults Aged 70 and Older: A Randomized Clinical Trial. *Front Aging, 3*, 852643. doi: 10.3389/fragi.2022.852643

[22] Lin, C., Salzillo, T. C., Bader, D. A., Wilkenfeld, S. R., Awad, D., Pulliam, T. L., . . . Frigo, D. E. (2019). Prostate Cancer Energetics and Biosynthesis. *Adv Exp Med Biol, 1210*, 185-237. doi: 10.1007/978-3-030-32656-2_10

[23] Liu, Y. (2006). Fatty acid oxidation is a dominant bioenergetic pathway in prostate cancer. *Prostate Cancer Prostatic Dis, 9*(3), 230-234. doi: 10.1038/sj.pcan.4500879

[24] Pietrocola, F., Galluzzi, L., Bravo-San Pedro, J. M., Madeo, F., & Kroemer, G. (2015). Acetyl coenzyme A: a central metabolite and second messenger. *Cell Metab, 21*(6), 805-821. doi: 10.1016/j.cmet.2015.05.014

[25] Jiang, Y., He, C., Ye, H., Xu, Q., Chen, X., Chen, Y., . . . Wang, M. (2023). Comprehensive analysis of the lysine succinylome in fish oil-treated prostate cancer cells. *Life Sci Alliance, 6*(11). doi: 10.26508/lsa.202302131

[26] Ritchie, M. E., Phipson, B., Wu, D., Hu, Y., Law, C. W., Shi, W., & Smyth, G. K. (2015). limma powers differential expression analyses for RNA-sequencing and microarray studies. *Nucleic Acids Res, 43*(7), e47. doi: 10.1093/nar/gkv007

[27] Wu, T., Hu, E., Xu, S., Chen, M., Guo, P., Dai, Z., . . . Yu, G. (2021). clusterProfiler 4.0: A universal enrichment tool for interpreting omics data. *Innovation (Camb), 2*(3), 100141. doi: 10.1016/j.xinn.2021.100141

[28] Cheng, Y. J., Zhu, Z. X., Zhou, J. S., Hu, Z. Q., Zhang, J. P., Cai, Q. P., & Wang, L. H. (2015). Silencing profilin-1 inhibits gastric cancer progression via integrin beta1/focal adhesion kinase pathway modulation. *World J Gastroenterol, 21*(8), 2323-2335. doi: 10.3748/wjg.v21.i8.2323

[29] Vitali, E., Franceschini, B., Milana, F., Soldani, C., Polidoro, M. A., Carriero, R., . . . Donadon, M. (2023). Filamin A is involved in human intrahepatic cholangiocarcinoma aggressiveness and progression. *Liver Int*. doi: 10.1111/liv.15800

[30] Di Donato, M., Giovannelli, P., Barone, M. V., Auricchio, F., Castoria, G., & Migliaccio, A. (2021). A Small Peptide Targeting the Ligand-Induced Androgen Receptor/Filamin a Interaction Inhibits the Invasive Phenotype of Prostate Cancer Cells. *Cells, 11*(1). doi: 10.3390/cells11010014

[31] Welter, H., Herrmann, C., Frohlich, T., Flenkenthaler, F., Eubler, K., Schorle, H., . . . Muller-Taubenberger, A. (2020). Filamin A Orchestrates Cytoskeletal Structure, Cell Migration and Stem Cell Characteristics in Human Seminoma TCam-2 Cells. *Cells, 9*(12). doi: 10.3390/cells9122563

[32] Ma, Y., Temkin, S. M., Hawkridge, A. M., Guo, C., Wang, W., Wang, X. Y., & Fang, X. (2018). Fatty acid oxidation: An emerging facet of metabolic transformation in cancer. *Cancer Lett, 435*, 92-100. doi: 10.1016/j.canlet.2018.08.006

[33] Xing, S., & Poirier, Y. (2012). The protein acetylome and the regulation of metabolism. *Trends Plant Sci, 17*(7), 423-430. doi: 10.1016/j.tplants.2012.03.008

[34] Houten, S. M., Violante, S., Ventura, F. V., & Wanders, R. J. (2016). The Biochemistry and Physiology of Mitochondrial Fatty Acid beta-Oxidation and Its Genetic Disorders. *Annu Rev Physiol, 78*, 23-44. doi: 10.1146/annurev-physiol-021115-105045

[35] Su, C. C., Yu, C. C., Shih, Y. W., Liu, K. L., Chen, H. W., Wu, C. C., . . . Li, C. C. (2023). Protective Effect of Alpha-Linolenic Acid on Human Oral Squamous Cell Carcinoma Metastasis and Apoptotic Cell Death. *Nutrients, 15*(23). doi: 10.3390/nu15234992

[36] Yin, H., Liu, Y., Yue, H., Tian, Y., Dong, P., Xue, C., . . . Wang, J. (2022). DHA- and EPA-Enriched Phosphatidylcholine Suppress Human Lung Carcinoma 95D Cells Metastasis via Activating the Peroxisome Proliferator-Activated Receptor gamma. *Nutrients, 14*(21). doi: 10.3390/nu14214675

[37] Onder, E., Cil, N., Secme, M., & Mete, G. A. (2024). Effect of alpha lipoic acid on epithelial mesenchymal transition in SKOV-3 cells. *Gene, 892*, 147880. doi: 10.1016/j.gene.2023.147880

[38] Fan, H., Huang, W., Guo, Y., Ma, X., & Yang, J. (2022). alpha-Linolenic Acid Suppresses Proliferation and Invasion in Osteosarcoma Cells via Inhibiting Fatty Acid Synthase. *Molecules, 27*(9). doi: 10.3390/molecules27092741

[39] Alkam, D., Feldman, E. Z., Singh, A., & Kiaei, M. (2017). Profilin1 biology and its mutation, actin(g) in disease. *Cell Mol Life Sci, 74*(6), 967-981. doi: 10.1007/s00018-016-2372-1

[40] Schutt, C. E., Myslik, J. C., Rozycki, M. D., Goonesekere, N. C., & Lindberg, U. (1993). The structure of crystalline profilin-beta-actin. *Nature, 365*(6449), 810-816. doi: 10.1038/365810a0

[41] Zhou, J., Kang, X., An, H., Lv, Y., & Liu, X. (2021). The function and pathogenic mechanism of filamin A. *Gene, 784*, 145575. doi: 10.1016/j.gene.2021.145575

[42] Ehrlicher, A. J., Nakamura, F., Hartwig, J. H., Weitz, D. A., & Stossel, T. P. (2011). Mechanical strain in actin networks regulates FilGAP and integrin binding to filamin A. *Nature, 478*(7368), 260-263. doi: 10.1038/nature10430

[43] Nakamura, F., Stossel, T. P., & Hartwig, J. H. (2011). The filamins: organizers of cell structure and function. *Cell Adh Migr, 5*(2), 160-169. doi: 10.4161/cam.5.2.14401

[44] Chen, H., Zhu, X., Cong, P., Sheetz, M. P., Nakamura, F., & Yan, J. (2011). Differential mechanical stability of filamin A rod segments. *Biophys J, 101*(5), 1231-1237. doi: 10.1016/j.bpj.2011.07.028

[45] Frantzi, M., Klimou, Z., Makridakis, M., Zoidakis, J., Latosinska, A., Borras, D. M., . . . Vlahou, A. (2016). Silencing of Profilin-1 suppresses cell adhesion and tumor growth via predicted alterations in integrin and Ca2+ signaling in T24M-based bladder cancer models. *Oncotarget, 7*(43), 70750-70768. doi: 10.18632/oncotarget.12218

[46] Argenzio, E., Klarenbeek, J., Kedziora, K. M., Nahidiazar, L., Isogai, T., Perrakis, A., . . . Innocenti, M. (2018). Profilin binding couples chloride intracellular channel protein CLIC4 to RhoA-mDia2 signaling and filopodium formation. *J Biol Chem, 293*(50), 19161-19176. doi: 10.1074/jbc.RA118.002779

[47] Jiang, C., Ding, Z., Joy, M., Chakraborty, S., Kim, S. H., Bottcher, R., . . . Roy, P. (2017). A balanced level of profilin-1 promotes stemness and tumor-initiating potential of breast cancer cells. *Cell Cycle, 16*(24), 2366-2373. doi: 10.1080/15384101.2017.1346759

[48] Chakraborty, S., Jiang, C., Gau, D., Oddo, M., Ding, Z., Vollmer, L., . . . Roy, P. (2018). Profilin-1 deficiency leads to SMAD3 upregulation and impaired 3D outgrowth of breast cancer cells. *Br J Cancer, 119*(9), 1106-1117. doi: 10.1038/s41416-018-0284-6

[49] Huang, Y., Sun, H., Ma, X., Zeng, Y., Pan, Y., Yu, D., . . . Xiang, Y. (2020). HLA-F-AS1/miR-330-3p/PFN1 axis promotes colorectal cancer progression. *Life Sci, 254*, 117180. doi: 10.1016/j.lfs.2019.117180

[50] George, L., Winship, A., Sorby, K., Dimitriadis, E., & Menkhorst, E. (2020). Profilin-1 is dysregulated in endometroid (type I) endometrial cancer promoting cell proliferation

and inhibiting pro-inflammatory cytokine production. *Biochem Biophys Res Commun, 531*(4), 459-464. doi: 10.1016/j.bbrc.2020.07.123

[51] Shao, Q. Q., Zhang, T. P., Zhao, W. J., Liu, Z. W., You, L., Zhou, L., . . . Zhao, Y. P. (2016). Filamin A: Insights into its Exact Role in Cancers. *Pathol Oncol Res, 22*(2), 245-252. doi: 10.1007/s12253-015-9980-1

[52] Savoy, R. M., & Ghosh, P. M. (2013). The dual role of filamin A in cancer: can't live with (too much of) it, can't live without it. *Endocr Relat Cancer, 20*(6), R341-356. doi: 10.1530/ERC-13-0364

## Figure legends

**Figure 1.** Global acetylomics study after the treatment of OA or EPA. (A) The cellular acetyl-CoA level changes after the treatment with ethanol, OA (100 μM) or EPA (100 μM) in PC-3 and LNCaP cells. Cells were treated for 24 h. The concentration was normalized with cell number. Three technical replicates were performed. (B) The workflow of the acetylomics study. Four batches of cells were harvested for analysis. (C) The number of identified peptides, regulated peptides and candidates. Peptides with a *p*-value less than 0.05 and at least in one comparison group among EPA vs. Ethanol, OA vs. Ethanol or EPA vs. OA were considered as regulated peptides. Peptides with a fold-change higher than 1.5 between EPA- and OA-treated groups were considered candidates. (D) Volcano plots of identified peptides. The protein names and acetylation sites of some candidates are presented. (E) Gene Ontology (GO) enrichment of all candidates. The data are presented as mean ± standard deviation. $^{**}p < 0.01$, $^{***}p < 0.001$.

**Figure 2.** Validation of PFN1 and FLNA acetylation. The mass spectra of the acetylated peptides of PFN1 and FLNA are shown in (A) and (B), respectively. Western blot validation of the PFN1 acetylation and FLNA acetylation are shown in (C) and (D), respectively. Cells were treated with ethanol, OA (100 μM), or EPA (100 μM) for 24 h. Anti-lysine acetylation motif antibody was used. Immunoblotting was repeated three times for each candidate. The data are presented as mean ± standard deviation. $^{*}p < 0.05$, $^{**}p < 0.01$, $^{***}p < 0.001$, ns = not significant.

**Figure 3.** PFN1 and FLNA are essential for the migration and invasion of prostate cancer cells. The mRNA and protein levels of PFN1 and FLNA in PC-3 or LNCaP cells after down-regulation are shown in (A) and (B) for PC-3 cells, (C) and (D) for

LNCaP cells, respectively. (E) Wound-healing assay for the migration of the prostate cancer cells. Cells were seeded and attached. After the wound was made by mechanical scratching, cells were washed with PBS and supplied with media without FBS. The scale bar indicates a length of 200 μm. (F) Transwell invasion assay. The upper chamber was pre-coated with Matrigel. The same number of cells were seeded in FBS-free media. The lower chamber contains media with 20% FBS. The scale bar indicates the length of 50 μm. The data are presented as mean ± standard deviation. *$p < 0.05$, **$p < 0.01$, ***$p < 0.001$.

**Figure 4.** OA stimulates while EPA impedes the migration and invasion of prostate cancer cells. (A) Wound-healing assay for the migration of prostate cancer cells. Cells were seeded and attached. After the wound was made by mechanical scratching, ethanol, OA (100 μM) or EPA (100 μM) were added. The scale bar indicates a length of 200 μm. (B) Transwell invasion assay. Cells were pre-treated with ethanol, OA (100 μM) or EPA (100 μM) for 24h and harvested. The same number of cells were seeded in the upper chamber pre-coated with Matrigel. The scale bar indicates a length of 50 μm. The data are presented as mean ± standard deviation. *$p < 0.05$, **$p < 0.01$, ***$p < 0.001$.

**Figure 5.** Immunofluorescence assay of F-actin with PFN1 or FLNA after treatment. The co-localization of F-actin with PFN1 (A & C) or FLNA (B & D) in PC-3 cells and LNCaP cells, respectively. The scale bar indicates the length of 10 μm. The bar chart indicates the percentage of PFN1 or FLNA localized to lamellipodia (PC-3) or filopodia (LNCaP). Three views for PC-3 cells and five for LNCaP were evaluated (please see supplementary figures). The data are presented as mean ± standard deviation. *$p < 0.05$, **$p < 0.01$, ***$p < 0.001$, ns = not significant.

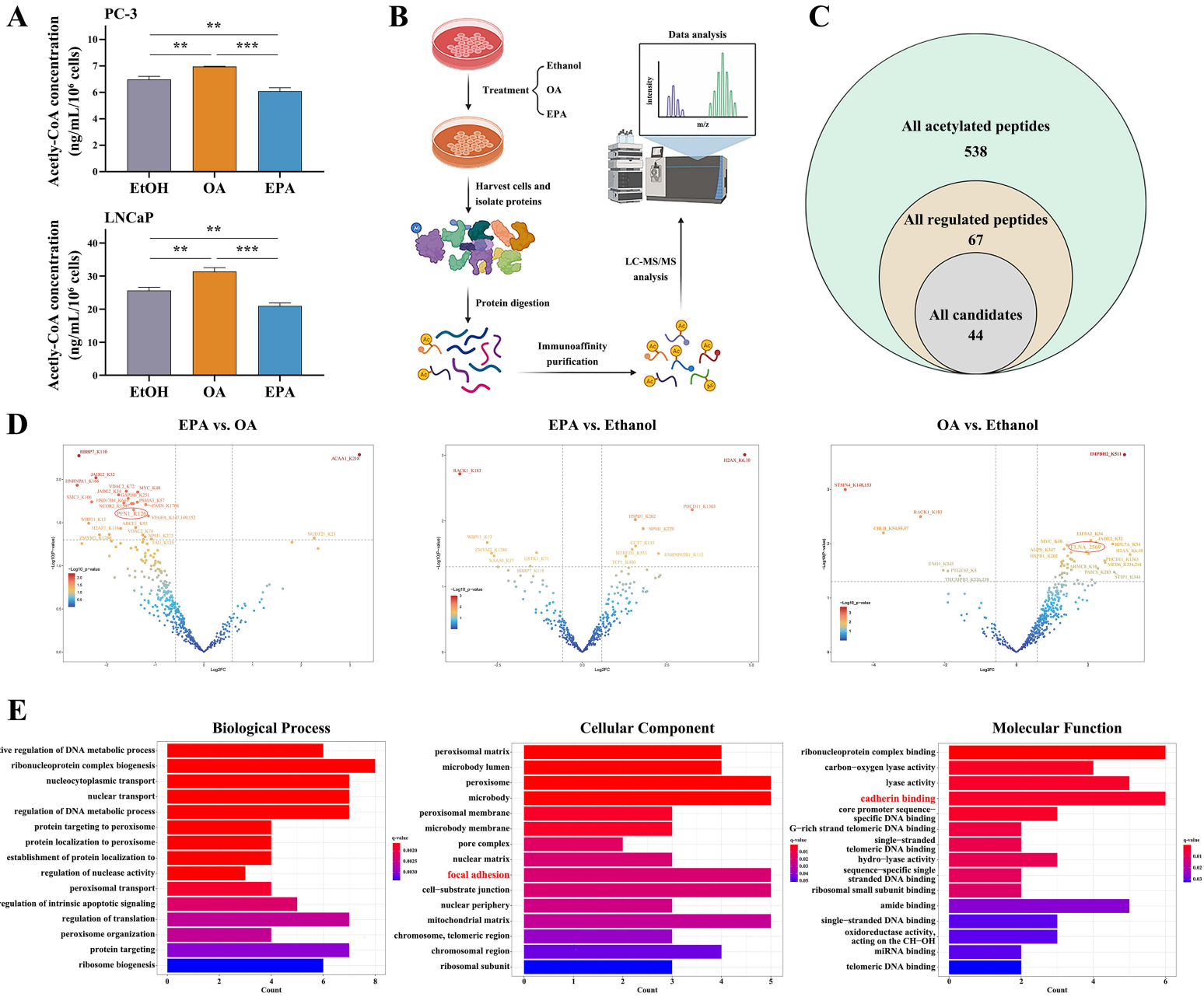


**Figure 1.** Global acetylomics study after the treatment of OA or EPA. (A) The cellular acetyl-CoA level changes after the treatment with ethanol, OA (100 μM) or EPA (100 μM) in PC-3 and LNCaP cells. Cells were treated for 24 h. The concentration was normalized with cell number. Three technical replicates were performed. (B) The workflow of the acetylomics study. Four batches of cells were harvested for analysis. (C) The number of identified peptides, regulated peptides and candidates. Peptides with a *p*-value less than 0.05 and at least in one comparison group among EPA vs. Ethanol, OA vs. Ethanol or EPA vs. OA were considered as regulated peptides. Peptides with a fold-change higher than 1.5 between EPA- and OA-treated groups were considered candidates. (D) Volcano plots of identified peptides. The protein names and acetylation sites of some candidates are presented. (E) Gene Ontology (GO) enrichment of all candidates. The data are presented as mean ± standard deviation. $^{**}p < 0.01$, $^{***}p < 0.001$.

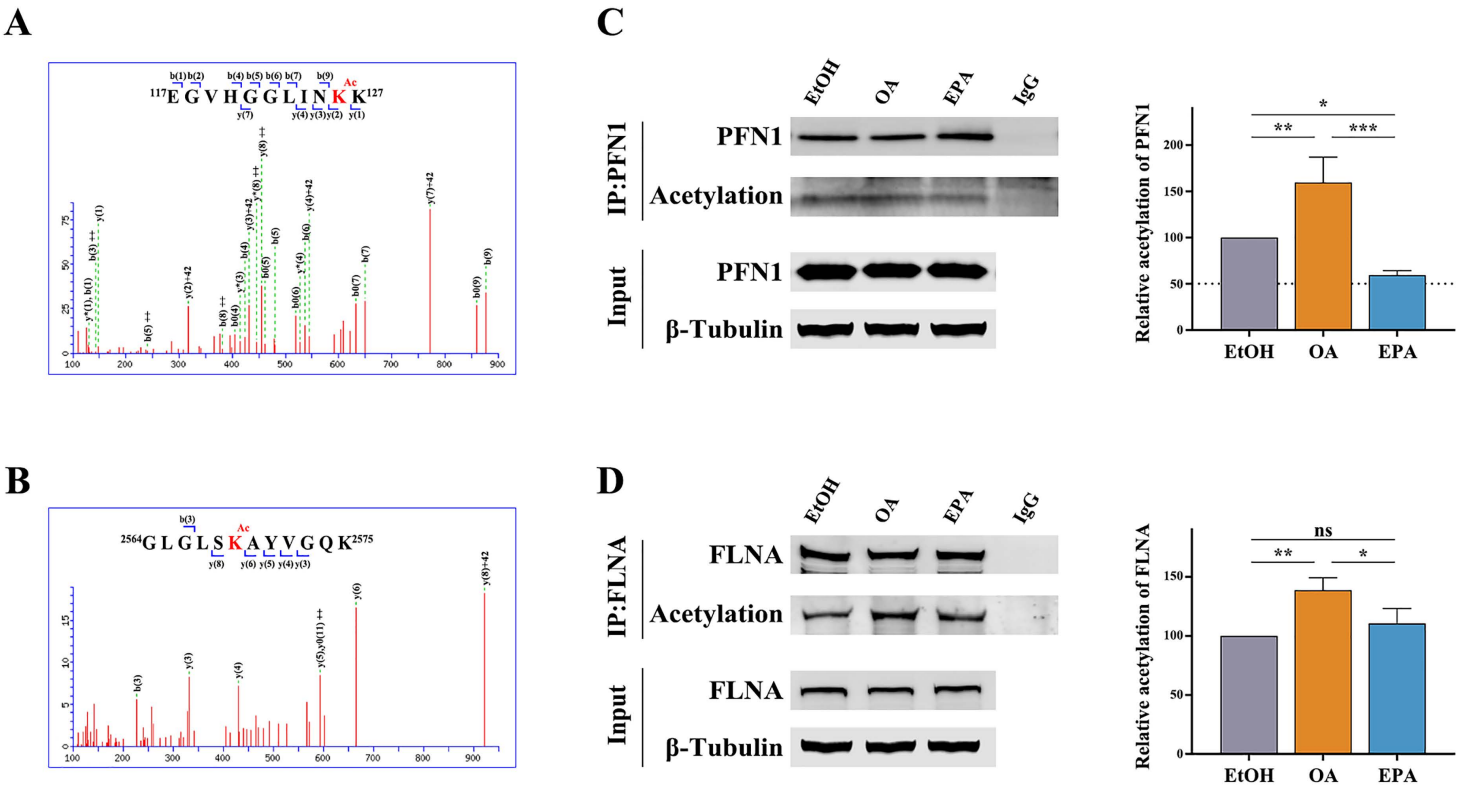


**Figure 2.** Validation of PFN1 and FLNA acetylation. The mass spectra of the acetylated peptides of PFN1 and FLNA are shown in (A) and (B), respectively. Western blot validation of the PFN1 acetylation and FLNA acetylation are shown in (C) and (D), respectively. Cells were treated with ethanol, OA (100 μM), or EPA (100 μM) for 24 h. Anti-lysine acetylation motif antibody was used. Immunoblotting was repeated three times for each candidate. The data are presented as mean ± standard deviation. *$p < 0.05$, **$p < 0.01$, ***$p < 0.001$, ns = not significant.

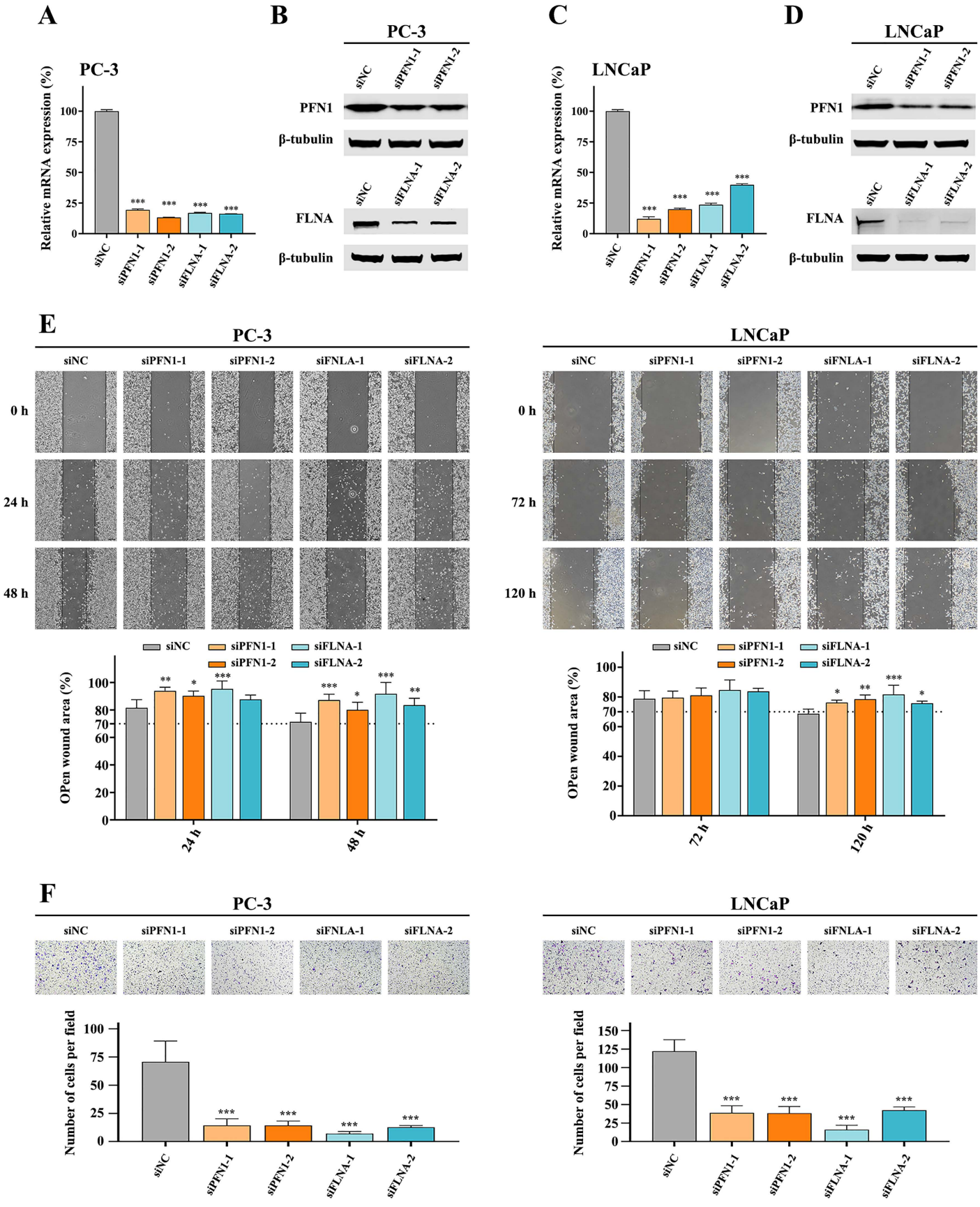


**Figure 3.** PFN1 and FLNA are essential for the migration and invasion of prostate cancer cells. The mRNA and protein levels of PFN1 and FLNA in PC-3 or LNCaP cells after down-regulation are shown in (A) and (B) for PC-3 cells, (C) and (D) for LNCaP cells, respectively. (E) Wound-healing assay for the migration of the prostate cancer cells. Cells were seeded and attached. After the wound was made by mechanical scratching, cells were washed with PBS and supplied with media without FBS. The scale bar indicates a length of 200 μm. (F) Transwell invasion assay. The upper chamber was pre-coated with Matrigel. The same number of cells were seeded in FBS-free media. The lower chamber contains media with 20% FBS. The scale bar indicates the length of 50 μm. The data are presented as mean ± standard deviation. $*p < 0.05$, $**p < 0.01$, $***p < 0.001$.

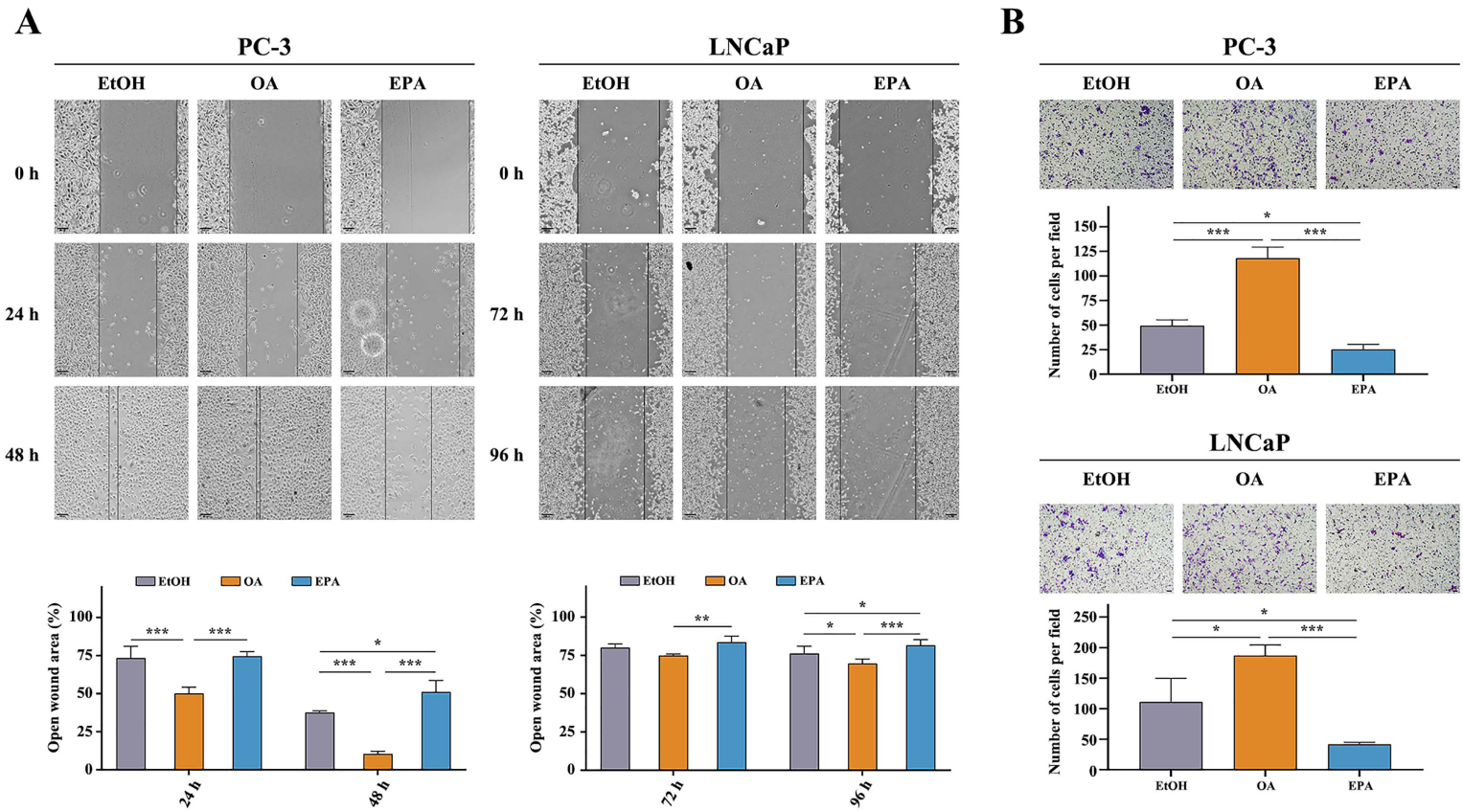


**Figure 4.** OA stimulates while EPA impedes the migration and invasion of prostate cancer cells. (A) Wound-healing assay for the migration of prostate cancer cells. Cells were seeded and attached. After the wound was made by mechanical scratching, ethanol, OA (100 μM) or EPA (100 μM) were added. The scale bar indicates a length of 200 μm. (B) Transwell invasion assay. Cells were pre-treated with ethanol, OA (100 μM) or EPA (100 μM) for 24h and harvested. The same number of cells were seeded in the upper chamber pre-coated with Matrigel. The scale bar indicates a length of 50 μm. The data are presented as mean ± standard deviation. *$p < 0.05$, **$p < 0.01$, ***$p < 0.001$.

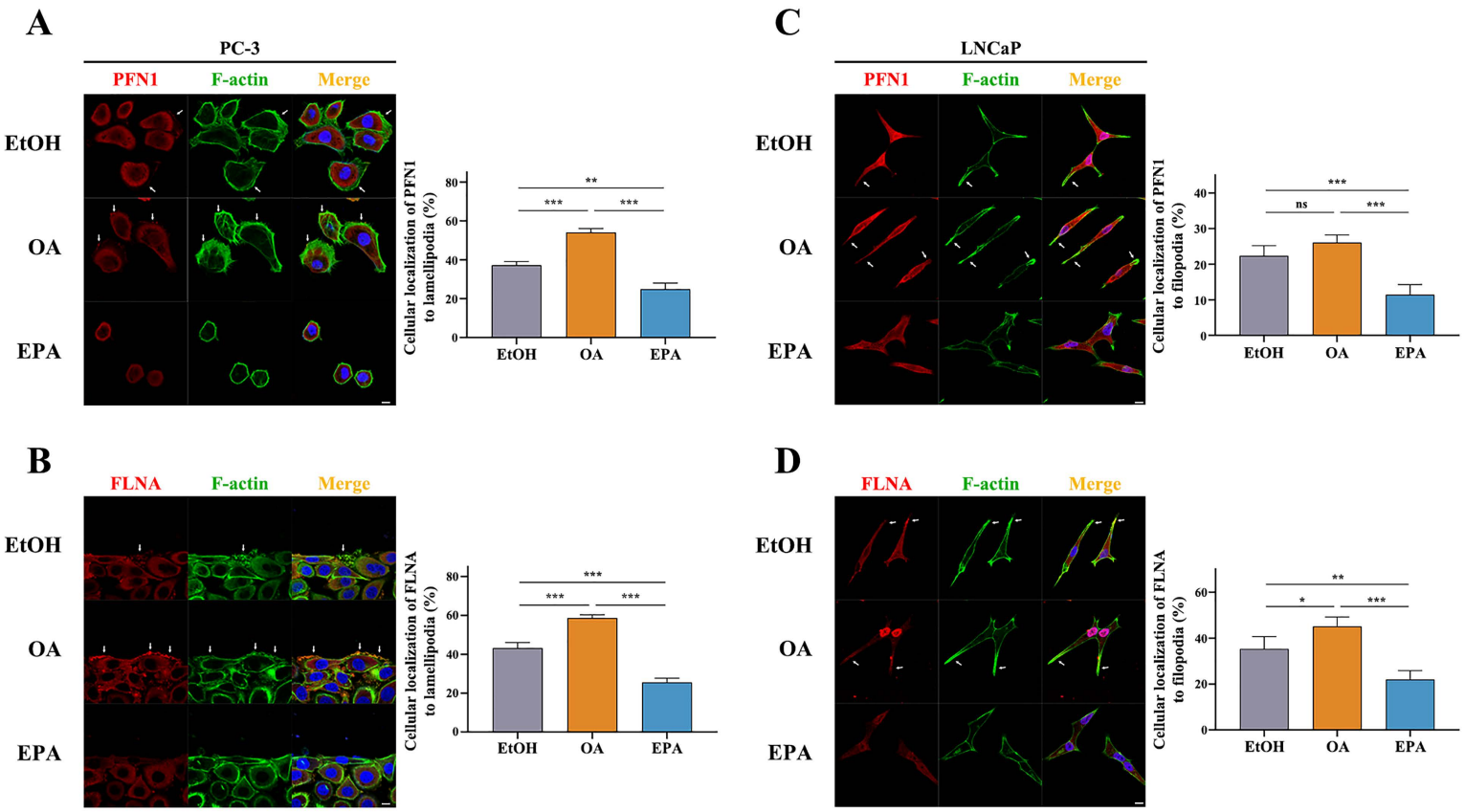


**Figure 5.** Immunofluorescence assay of F-actin with PFN1 or FLNA after treatment. The co-localization of F-actin with PFN1 (A & C) or FLNA (B & D) in PC-3 cells and LNCaP cells, respectively. The scale bar indicates the length of 10 μm. The bar chart indicates the percentage of PFN1 or FLNA localized to lamellipodia (PC-3) or filopodia (LNCaP). Three views for PC-3 cells and five for LNCaP were evaluated (please see supplementary figures). The data are presented as mean ± standard deviation. *$p < 0.05$, **$p < 0.01$, ***$p < 0.001$, ns = not significant.

# Supporting Information for

# Global acetylome profiling indicates EPA impedes but OA promotes prostate cancer motility through altered acetylation of PFN1 and FLNA

Chao He[1], Xiuyuan Chen[2], Ying Chen[1], Jianying Sun[1], Manting Qi[1], Sonia Rocha[3], Mu Wang[1,2*]

[1]Academy of Pharmacy, Xi'an Jiaotong-Liverpool University, Suzhou, Jiangsu 215123, China

[2] Department of Biological Sciences, Xi'an Jiaotong-Liverpool University, Suzhou, Jiangsu 215123, China

[3] Department of Molecular Physiology and Cell Signalling, Institute of Systems, Molecular and Integrative Biology, University of Liverpool, Liverpool L69 7ZB, United Kingdom

*Corresponding author: Prof. Mu Wang, PhD. E-mail: mu.wang@xjtlu.edu.cn.

**Table of Contents:**

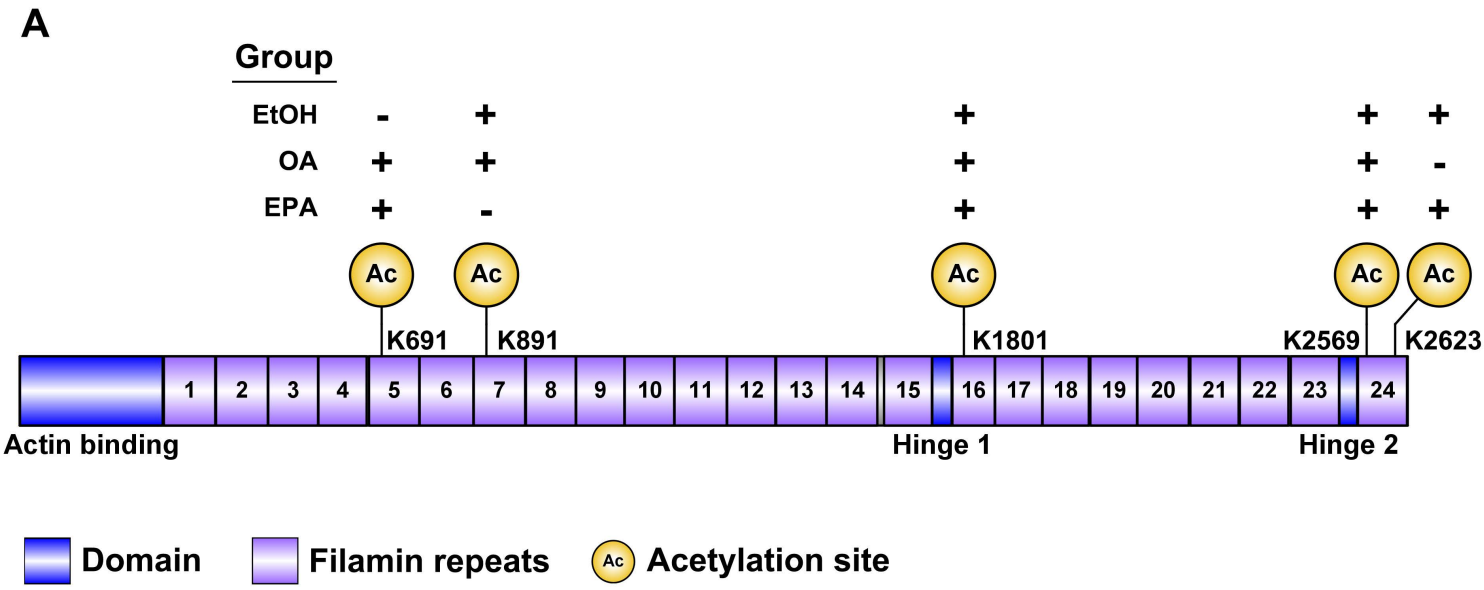


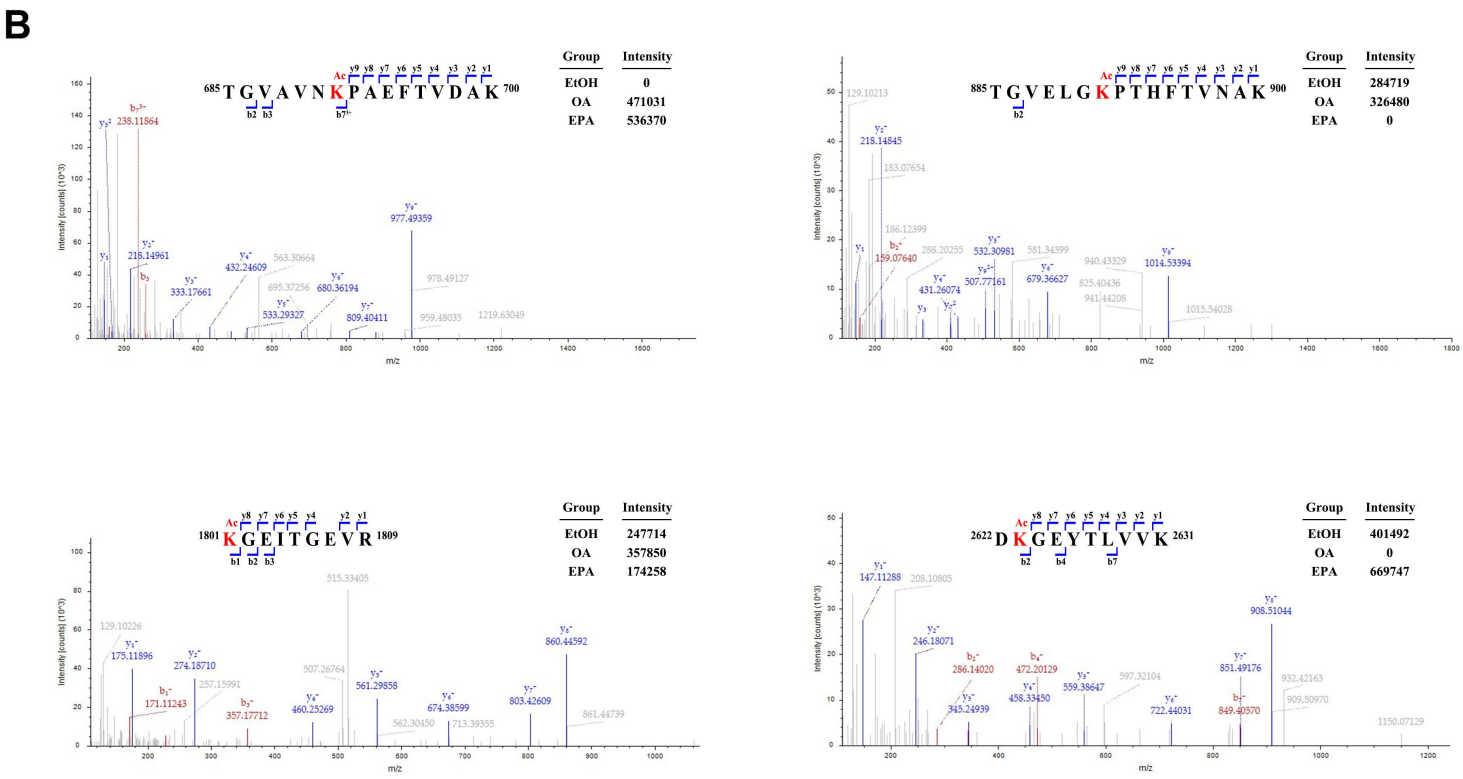


**Figure S1. Acetylation of FLNA in PC-3 cells.**

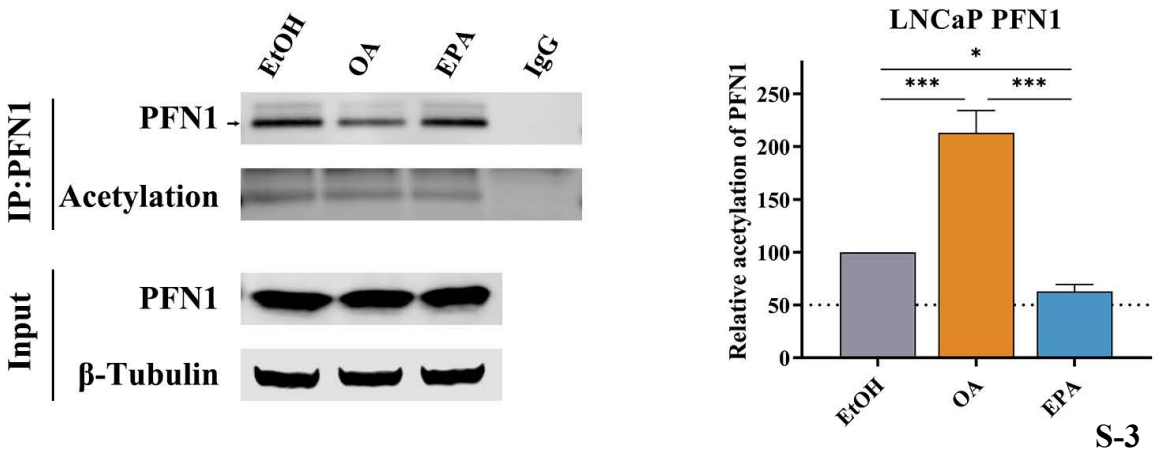


**Figure S2. Western blot validation of the acetylation of PFN1 after IP in LNCaP cells.**

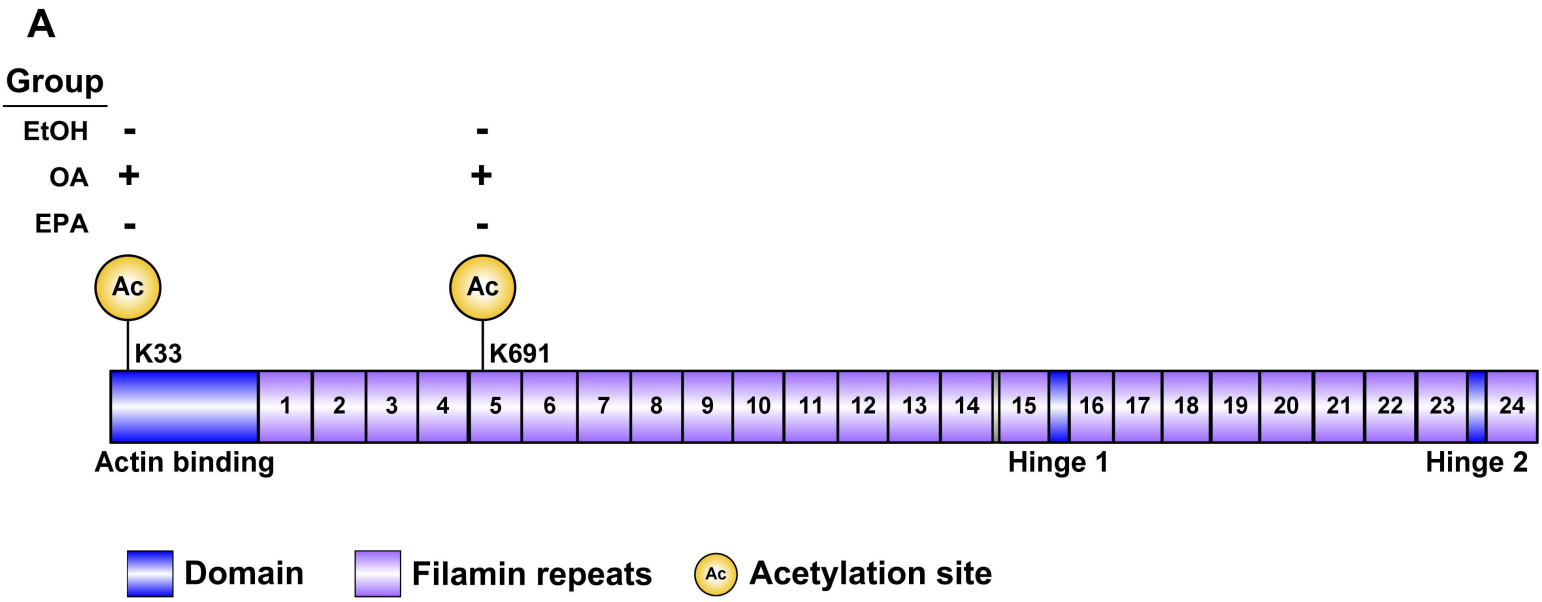


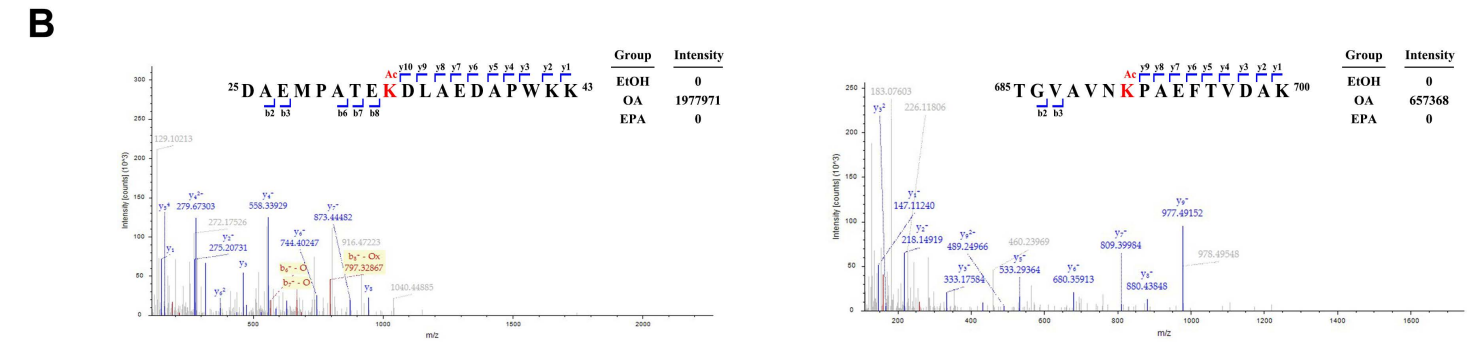


**Figure S3. Acetylation of FLNA in LNCaP cells.**

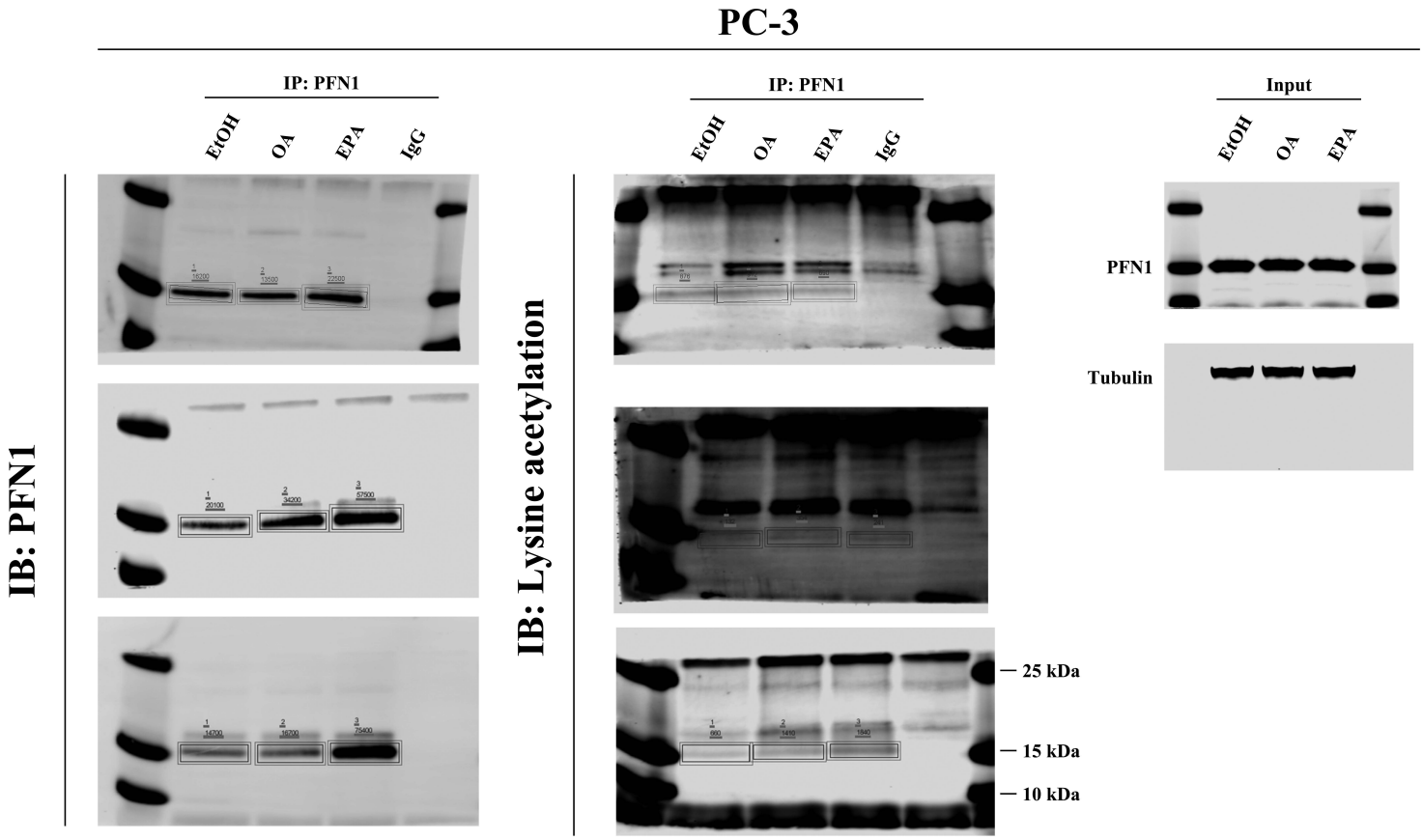


S-5

**Figure S4 Uncropped western blot images of Figure 2C**

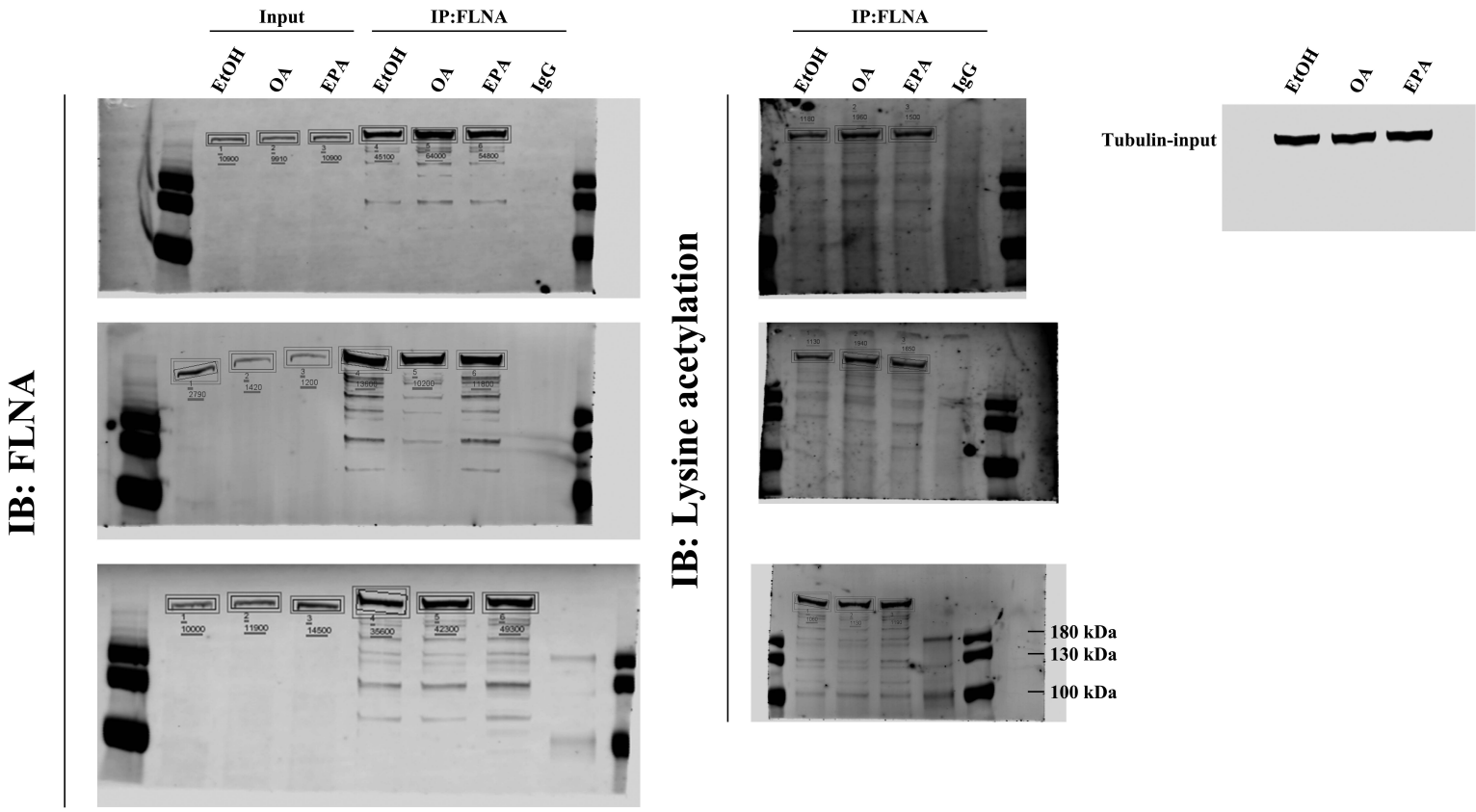




**Figure S5 Uncropped western blot images of Figure 2D**

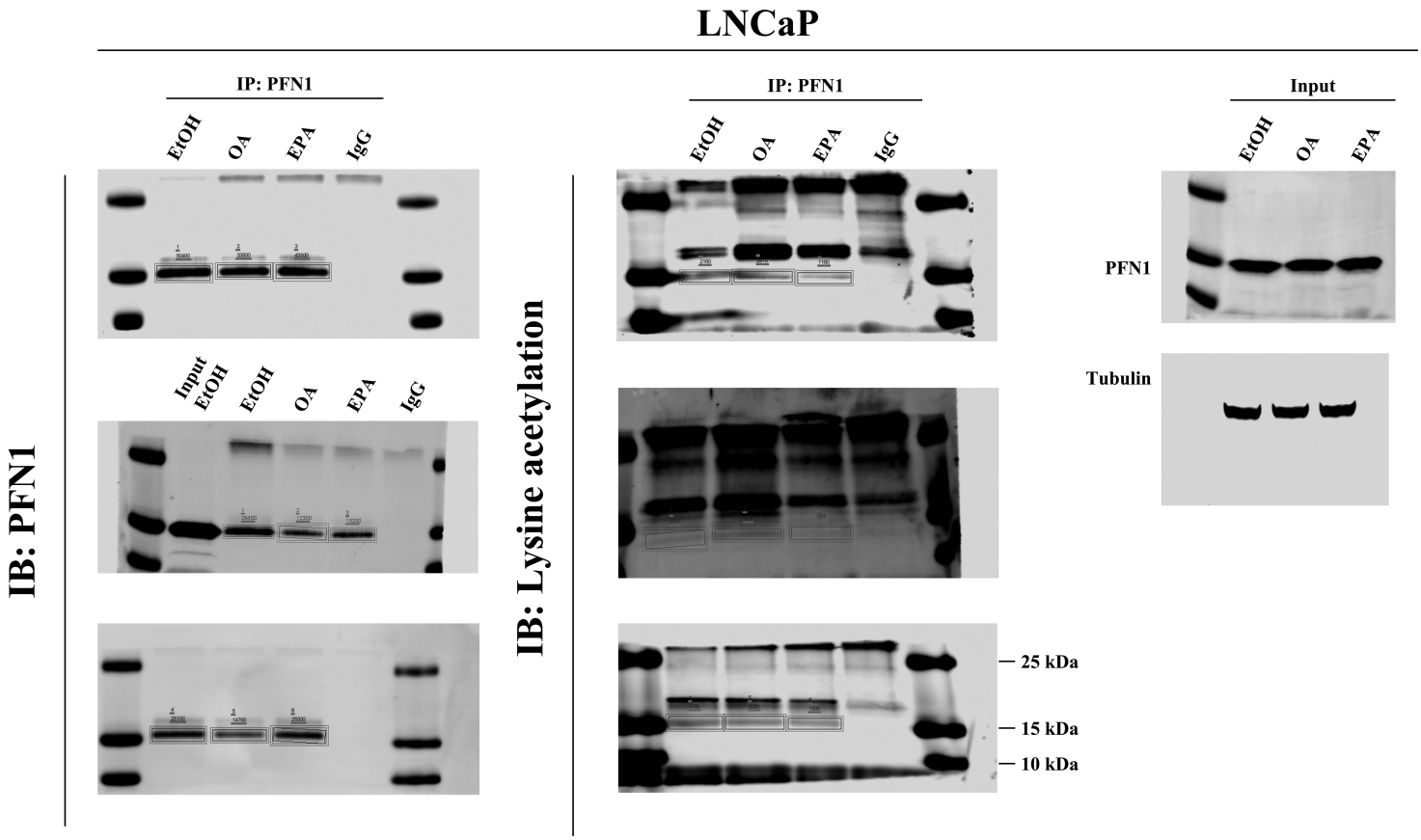


**Figure S6 Uncropped western blot images of Figure S2**

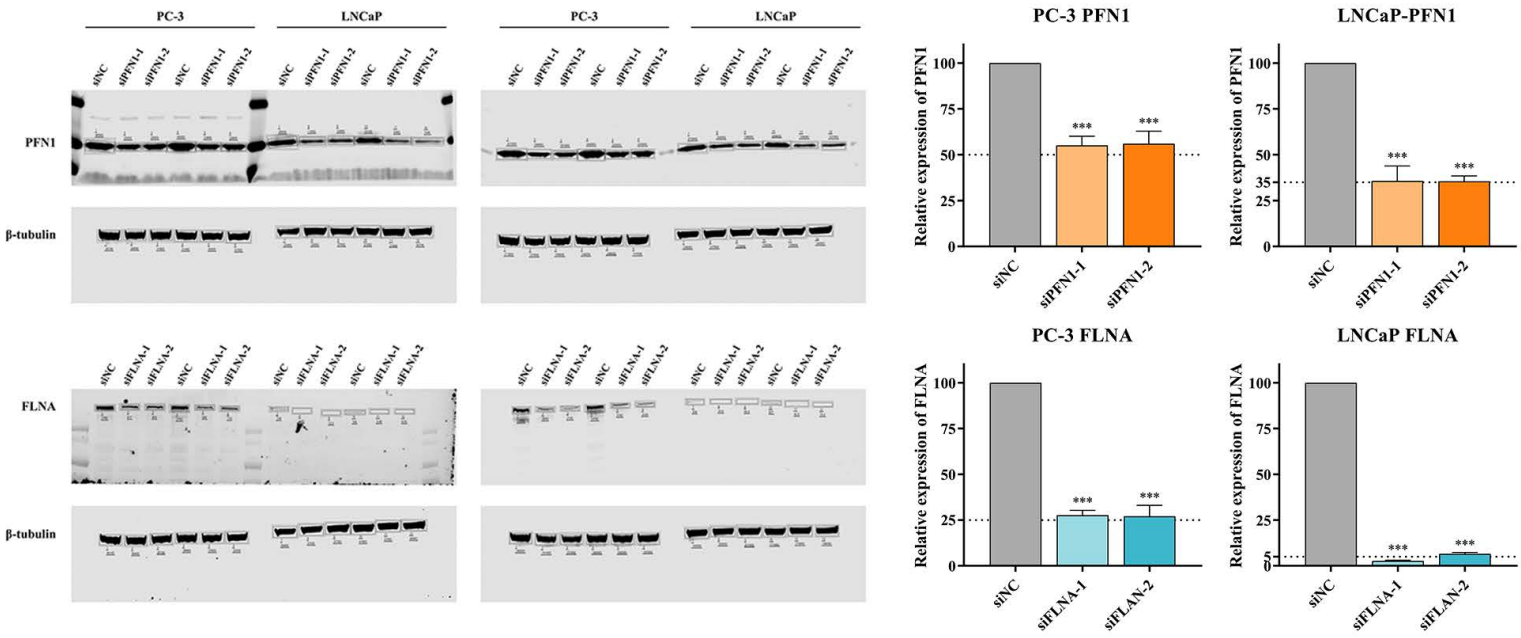




**Figure S7. Uncropped images and bar graph of Western blot after down-regulation of PFN1 or FLNA.**

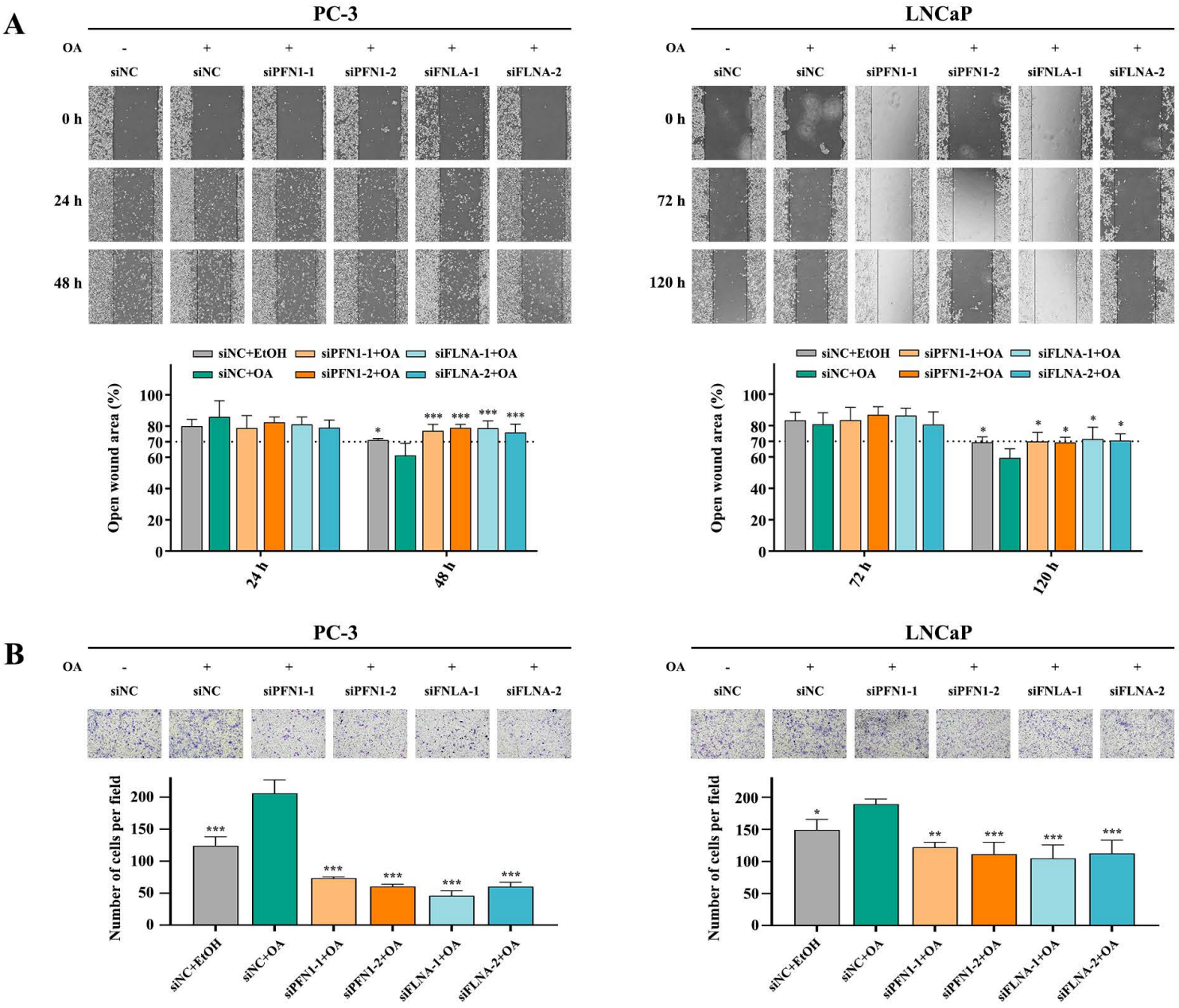


**Figure S8. Motility of PFN1 or FLNA down-regulated cells upon OA treatment**

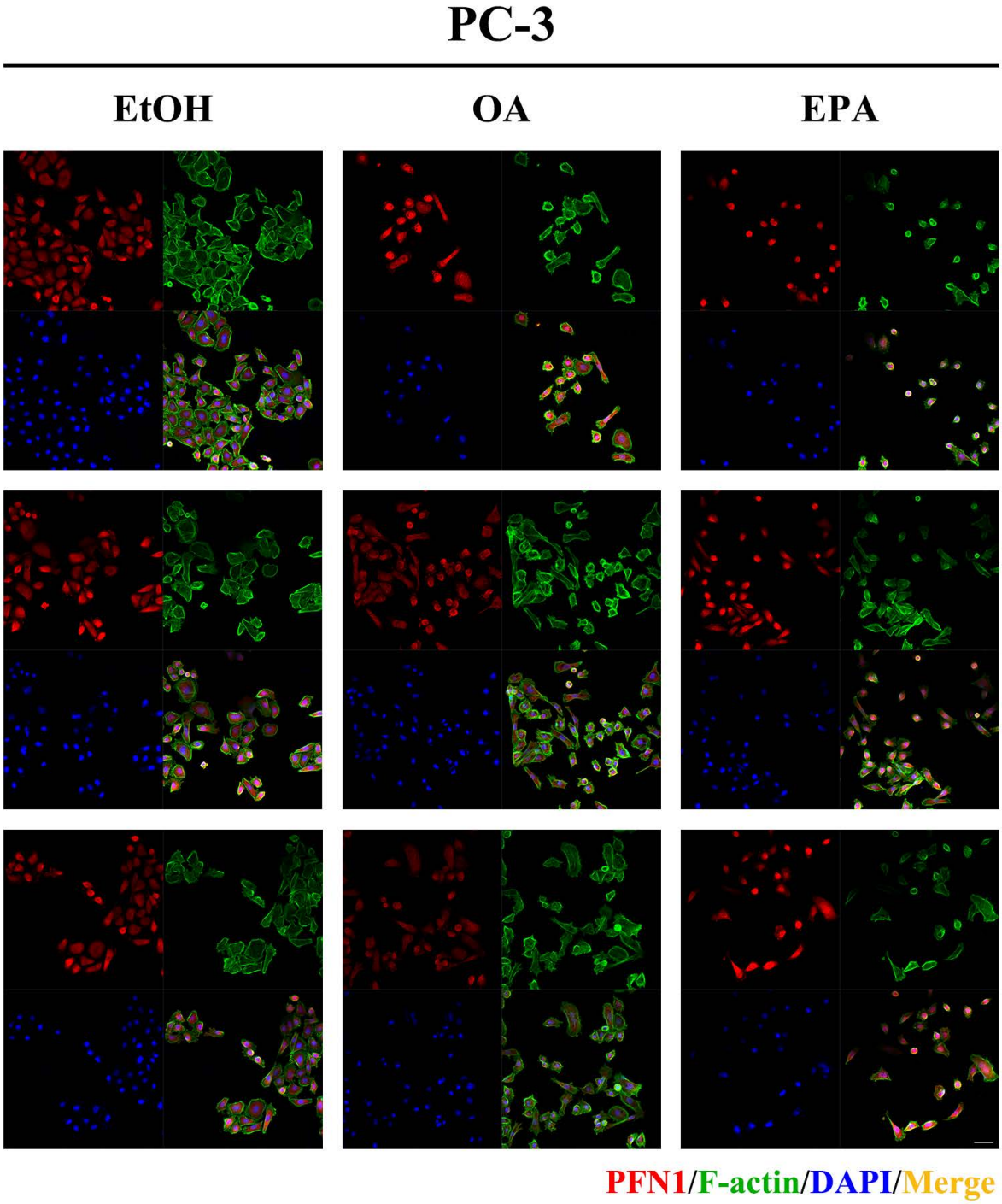


**Figure S9 The co-localization of F-actin with PFN1 in PC-3 cells**

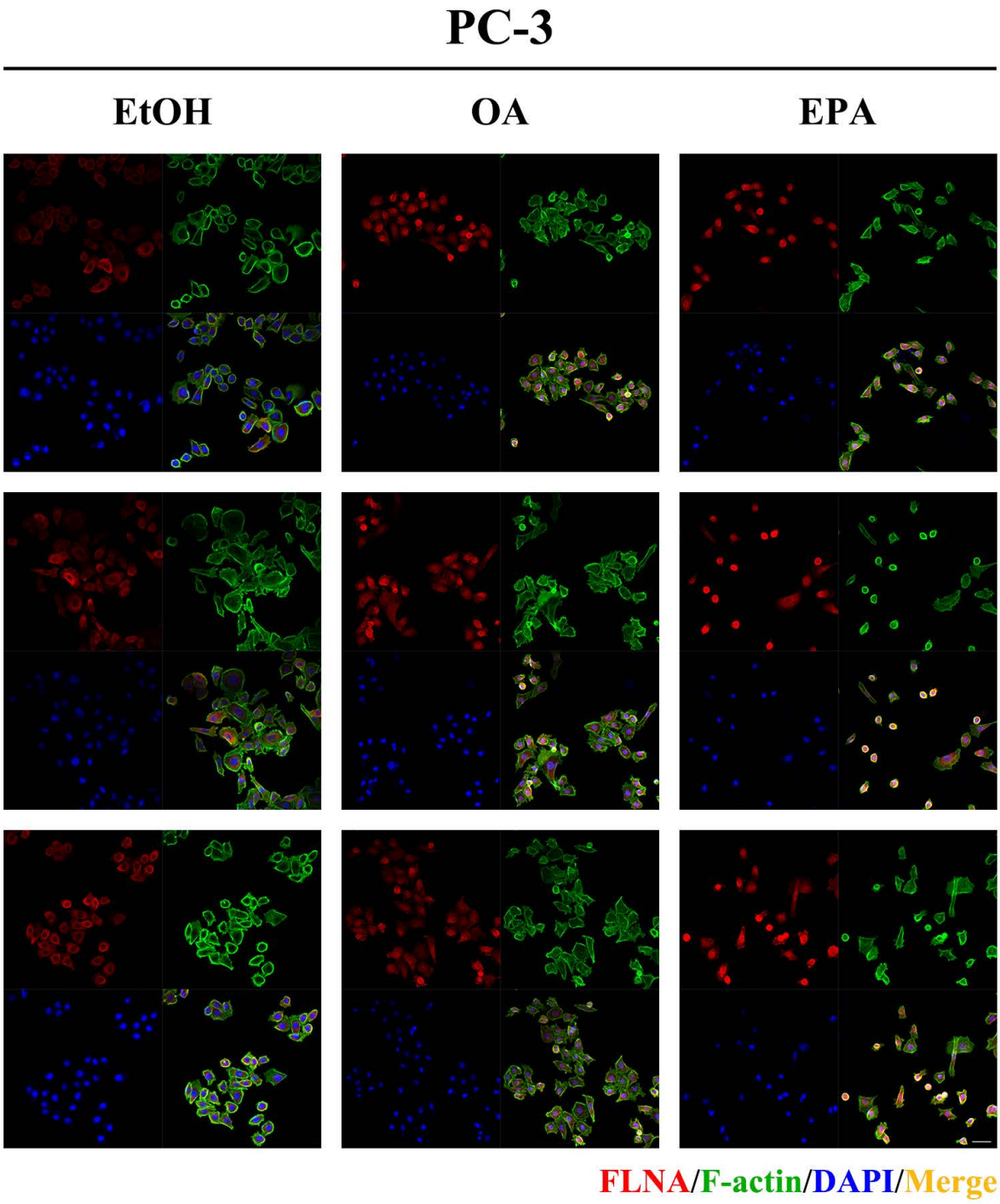


**Figure S10 The co-localization of F-actin with FLNA in PC-3 cells**

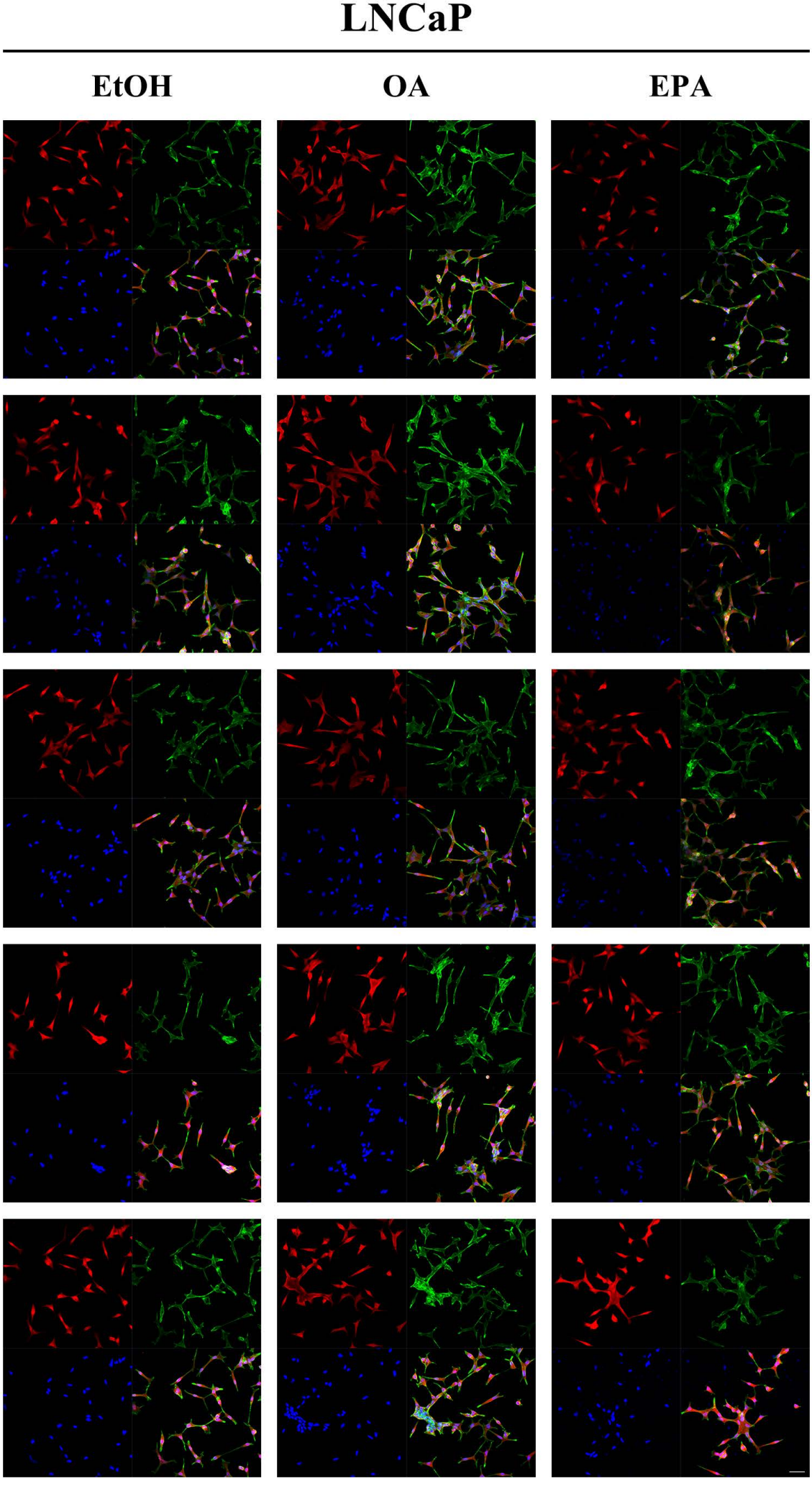


**Figure S11 The co-localization of F-actin with PFN1 in LNCaP cells**

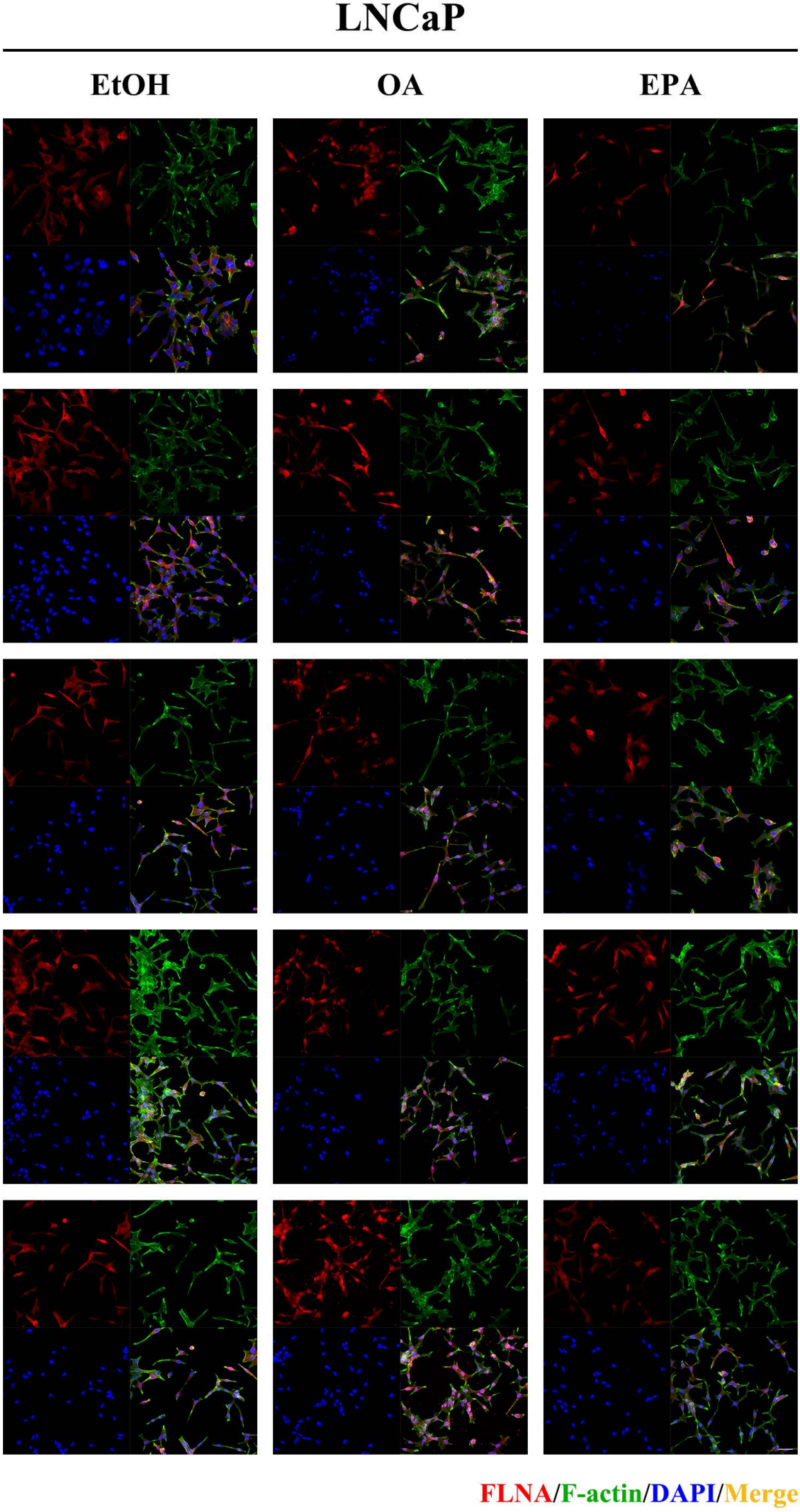


**Figure S12 The co-localization of F-actin with FLNA in LNCaP cells**

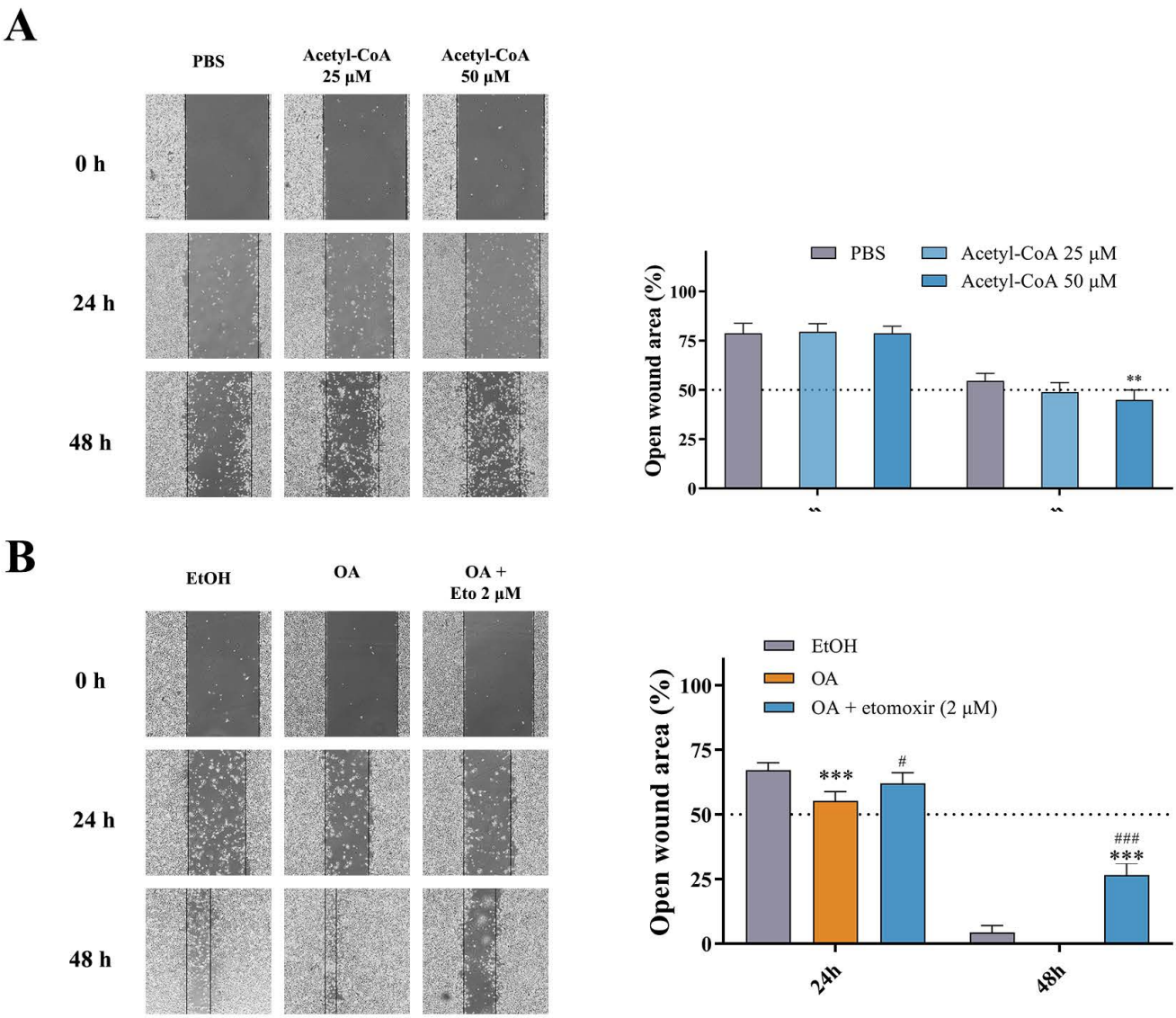


**Figure S13. Wound-healing of Acetyl-CoA or etomoxir treatment in PC-3 cells**

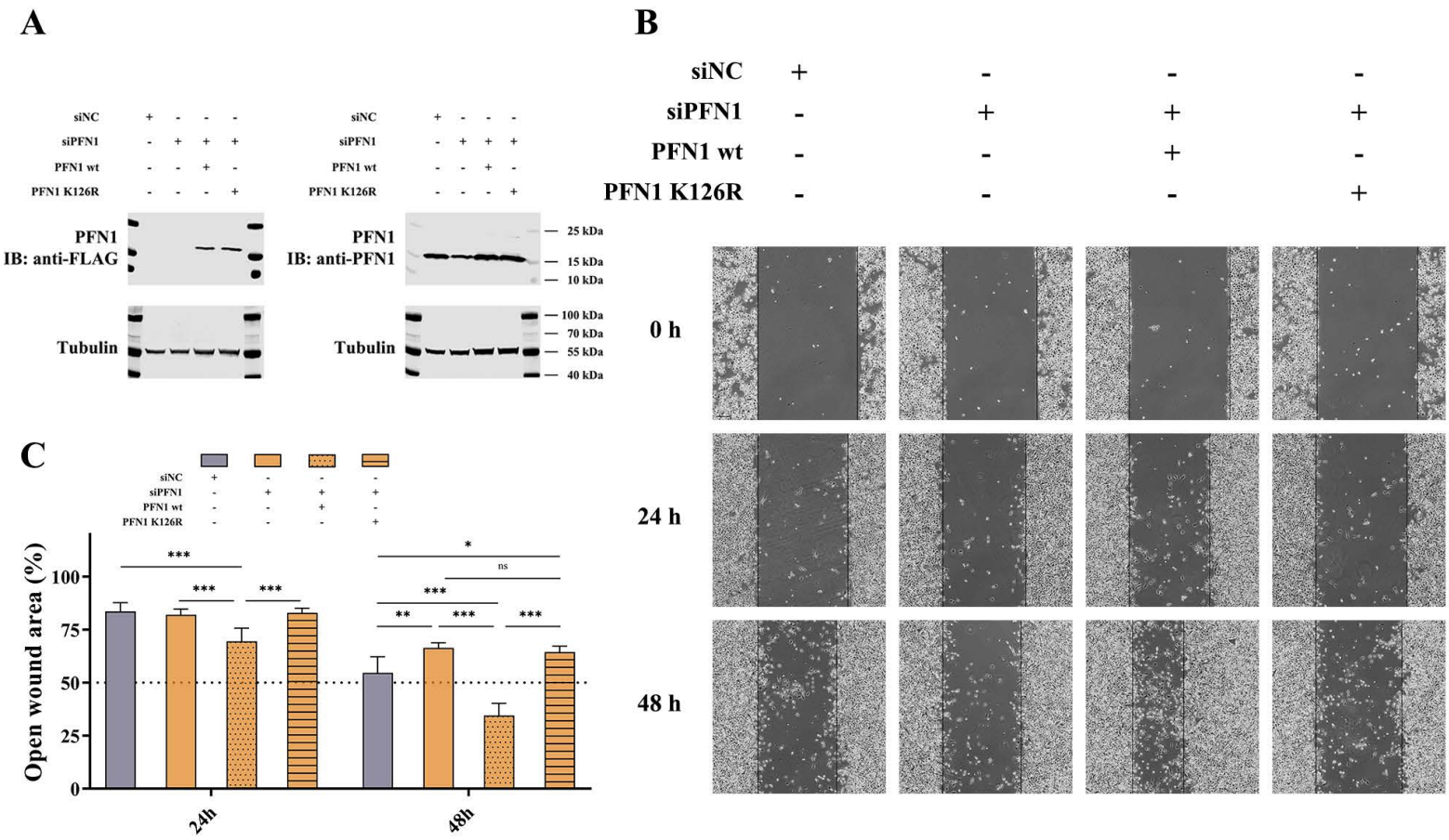


**Figure S14 Effect of PFN1-K126R mutation on the migration of PC-3 cells.** The RNA interference-resistant coding region of PFN1 wild-type or K126R containing synonymous mutation was amplified and cloned into pcDNA3.1 (+) vector (GenePharma)

# Table.S1 instrument settings for validation study

| Parameters | Settings |
|---|---|
| **General:** | |
| Runtime | 56 min |
| Polarity | Positive |
| Default charge state | 3 |
| **Full MS:** | |
| Resolution | 70,000 |
| AGC target | 3e6 |
| Maximum IT | 100 ms |
| Scan range | 400-1600 m/z |
| **dd-MS$^2$/dd-SIM:** | |
| Resolution | 17,500 |
| AGC target | 1e5 |
| Maximum IT | 50 ms |
| Loop count | 35 |
| Isolation window | 1.6 m/z |
| Fixed first mass | 110.0 m/z |
| (N)CE / stepped (N)CE | nce: 28 |
| Spectrum data type | Centroid |
| **dd settings:** | |
| Minimum AGC target | 8.00e3 |
| Intensity threshold | 1.6e5 |
| Exclude isotopes | on |
| Dynamic exclusion | 45.0 s |

## Table.S2 siRNAs for downregulation of candidates

| Target | siRNAs | |
|---|---|---|
| | Sense | Anti-sense |
| PFN1-1 | CCGGGUGGAACGCCUACAUTT | AUGUAGGCGUUCCACCCGGTT |
| PFN1-2 | GAAGGUGUCCACGGUGGUUTT | AACCACCGUGGACACCUUCTT |
| FLNA-1 | GCACUUACAGCUGCUCCUATT | UAGGAGCAGCUGUAAGUGCTT |
| FLNA-2 | GCUGGCAGCUACACCAUUATT | UAAUGGUGUAGCUGCCAGCTT |

## Table S3 Gene ontology enrichment of identified candidates

| ONTOLOGY | ID | Description | GeneRatio | BgRatio | pvalue | p.adjust | qvalue | geneID |
|---|---|---|---|---|---|---|---|---|
| BP | GO:0051054 | positive regulation of DNA metabolic process | 6/41 | 198/18862 | 4.11E-06 | 0.002421827 | 0.001630012 | HNRNPA1/MYC/RPS3/PTGES3/HNRNPA2B1/H2AX |
| BP | GO:0022613 | ribonucleoprotein complex biogenesis | 8/41 | 473/18862 | 6.80E-06 | 0.002421827 | 0.001630012 | WBP11/NOLC1/ABCE1/RPL7A/NPM1/PDCD11/PTGES3/NUDT21 |
| BP | GO:0006913 | nucleocytoplasmic transport | 7/41 | 340/18862 | 7.72E-06 | 0.002421827 | 0.001630012 | HNRNPA1/NOLC1/ABCE1/NPM1/FLNA/CBLB/HNRNPA2B1 |
| BP | GO:0051169 | nuclear transport | 7/41 | 343/18862 | 8.17E-06 | 0.002421827 | 0.001630012 | HNRNPA1/NOLC1/ABCE1/NPM1/FLNA/CBLB/HNRNPA2B1 |
| BP | GO:0051052 | regulation of DNA metabolic process | 7/41 | 353/18862 | 9.85E-06 | 0.002421827 | 0.001630012 | HNRNPA1/MYC/NPM1/RPS3/PTGES3/HNRNPA2B1/H2AX |
| BP | GO:0006625 | protein targeting to peroxisome | 4/41 | 68/18862 | 1.41E-05 | 0.002421827 | 0.001630012 | HSD17B4/SCP2/AGPS/GSTK1 |
| BP | GO:0072662 | protein localization to peroxisome | 4/41 | 68/18862 | 1.41E-05 | 0.002421827 | 0.001630012 | HSD17B4/SCP2/AGPS/GSTK1 |
| BP | GO:0072663 | establishment of protein localization to peroxisome | 4/41 | 68/18862 | 1.41E-05 | 0.002421827 | 0.001630012 | HSD17B4/SCP2/AGPS/GSTK1 |
| BP | GO:0032069 | regulation of nuclease activity | 3/41 | 22/18862 | 1.43E-05 | 0.002421827 | 0.001630012 | ABCE1/NPM1/RPS3 |
| BP | GO:0043574 | peroxisomal transport | 4/41 | 72/18862 | 1.78E-05 | 0.00271377 | 0.001826504 | HSD17B4/SCP2/AGPS/GSTK1 |
| BP | GO:2001242 | regulation of intrinsic apoptotic signaling pathway | 5/41 | 160/18862 | 2.42E-05 | 0.003355551 | 0.002258455 | VDAC2/ENO1/RACK1/RPS3/PPIF |
| BP | GO:0006417 | regulation of translation | 7/41 | 425/18862 | 3.25E-05 | 0.003842155 | 0.002585964 | NOLC1/GAPDH/NPM1/SRP9/RACK1/EIF5A2/RPS3 |
| BP | GO:0007031 | peroxisome organization | 4/41 | 84/18862 | 3.27E-05 | 0.003842155 | 0.002585964 | HSD17B4/SCP2/AGPS/GSTK1 |
| BP | GO:0006605 | protein targeting | 7/41 | 441/18862 | 4.12E-05 | 0.004492832 | 0.003023902 | HSD17B4/RPL7A/SRP9/SCP2/AGPS/RPS3/GSTK1 |
| BP | GO:0042254 | ribosome biogenesis | 6/41 | 307/18862 | 4.93E-05 | 0.00501977 | 0.003378558 | WBP11/NOLC1/ABCE1/RPL7A/NPM1/PDCD11 |
| BP | GO:0030224 | monocyte differentiation | 3/41 | 36/18862 | 6.48E-05 | 0.005670773 | 0.003816716 | MYC/FASN/VEGFA |
| BP | GO:0050657 | nucleic acid transport | 5/41 | 198/18862 | 6.68E-05 | 0.005670773 | 0.003816716 | HNRNPA1/ABCE1/NPM1/EIF5A2/HNRNPA2B1 |
| BP | GO:0050658 | RNA transport | 5/41 | 198/18862 | 6.68E-05 | 0.005670773 | 0.003816716 | HNRNPA1/ABCE1/NPM1/EIF5A2/HNRNPA2B1 |
| BP | GO:0051236 | establishment of RNA localization | 5/41 | 201/18862 | 7.17E-05 | 0.005768652 | 0.003882594 | HNRNPA1/ABCE1/NPM1/EIF5A2/HNRNPA2B1 |
| BP | GO:0034248 | regulation of cellular amide metabolic process | 7/41 | 494/18862 | 8.42E-05 | 0.00613616 | 0.004129945 | NOLC1/GAPDH/NPM1/SRP9/RACK1/EIF5A2/RPS3 |
| BP | GO:2000278 | regulation of DNA biosynthetic process | 4/41 | 107/18862 | 8.43E-05 | 0.00613616 | 0.004129945 | HNRNPA1/MYC/PTGES3/HNRNPA2B1 |
| BP | GO:0051972 | regulation of telomerase activity | 3/41 | 47/18862 | 0.000144633 | 0.009738275 | 0.00655435 | MYC/PTGES3/HNRNPA2B1 |
| BP | GO:0006403 | RNA localization | 5/41 | 234/18862 | 0.000146584 | 0.009738275 | 0.00655435 | HNRNPA1/ABCE1/NPM1/EIF5A2/HNRNPA2B1 |
| BP | GO:0008611 | ether lipid biosynthetic process | 2/41 | 10/18862 | 0.00020517 | 0.011504209 | 0.007742913 | FASN/AGPS |
| BP | GO:0032070 | regulation of deoxyribonuclease activity | 2/41 | 10/18862 | 0.00020517 | 0.011504209 | 0.007742913 | NPM1/RPS3 |
| BP | GO:0046504 | glycerol ether biosynthetic process | 2/41 | 10/18862 | 0.00020517 | 0.011504209 | 0.007742913 | FASN/AGPS |
| BP | GO:0097384 | cellular lipid biosynthetic process | 2/41 | 10/18862 | 0.00020517 | 0.011504209 | 0.007742913 | FASN/AGPS |
| BP | GO:0015931 | nucleobase-containing compound transport | 5/41 | 253/18862 | 0.00021081 | 0.011504209 | 0.007742913 | HNRNPA1/ABCE1/NPM1/EIF5A2/HNRNPA2B1 |
| BP | GO:0009150 | purine ribonucleotide metabolic process | 6/41 | 408/18862 | 0.000233877 | 0.01199205 | 0.008071254 | HSD17B4/GAPDH/ADSL/ENO1/FASN/IMPDH2 |
| BP | GO:0060009 | Sertoli cell development | 2/41 | 11/18862 | 0.000250418 | 0.01199205 | 0.008071254 | HSD17B4/FLNA |
| BP | GO:1901503 | ether biosynthetic process | 2/41 | 11/18862 | 0.000250418 | 0.01199205 | 0.008071254 | FASN/AGPS |
| BP | GO:0006405 | RNA export from nucleus | 4/41 | 142/18862 | 0.000251142 | 0.01199205 | 0.008071254 | HNRNPA1/ABCE1/NPM1/HNRNPA2B1 |
| BP | GO:0009259 | ribonucleotide metabolic process | 6/41 | 425/18862 | 0.000291206 | 0.013252878 | 0.008919855 | HSD17B4/GAPDH/ADSL/ENO1/FASN/IMPDH2 |
| BP | GO:0052548 | regulation of endopeptidase activity | 6/41 | 426/18862 | 0.000294894 | 0.013252878 | 0.008919855 | GAPDH/PSMA3/MYC/VEGFA/RACK1/RPS3 |
| BP | GO:0019693 | ribose phosphate metabolic process | 6/41 | 435/18862 | 0.000329771 | 0.014265497 | 0.009601399 | HSD17B4/GAPDH/ADSL/ENO1/FASN/IMPDH2 |
| BP | GO:0097193 | intrinsic apoptotic signaling pathway | 5/41 | 283/18862 | 0.000353454 | 0.014265497 | 0.009601399 | VDAC2/ENO1/RACK1/RPS3/PPIF |
| BP | GO:0036109 | alpha-linolenic acid metabolic process | 2/41 | 13/18862 | 0.00035416 | 0.014265497 | 0.009601399 | HSD17B4/SCP2 |
| BP | GO:0006163 | purine nucleotide metabolic process | 6/41 | 441/18862 | 0.00035477 | 0.014265497 | 0.009601399 | HSD17B4/GAPDH/ADSL/ENO1/FASN/IMPDH2 |
| BP | GO:2000573 | positive regulation of DNA biosynthetic process | 3/41 | 65/18862 | 0.000379183 | 0.014733737 | 0.009916548 | HNRNPA1/MYC/PTGES3 |
| BP | GO:0000723 | telomere maintenance | 4/41 | 161/18862 | 0.000404905 | 0.014733737 | 0.009916548 | HNRNPA1/MYC/PTGES3/HNRNPA2B1 |
| BP | GO:0000054 | ribosomal subunit export from nucleus | 2/41 | 14/18862 | 0.000412618 | 0.014733737 | 0.009916548 | ABCE1/NPM1 |
| BP | GO:0033750 | ribosome localization | 2/41 | 14/18862 | 0.000412618 | 0.014733737 | 0.009916548 | ABCE1/NPM1 |
| BP | GO:0052547 | regulation of peptidase activity | 6/41 | 455/18862 | 0.000418908 | 0.014733737 | 0.009916548 | GAPDH/PSMA3/MYC/VEGFA/RACK1/RPS3 |
| BP | GO:0051170 | import into nucleus | 4/41 | 163/18862 | 0.00042427 | 0.014733737 | 0.009916548 | HNRNPA1/NOLC1/FLNA/CBLB |
| BP | GO:0072521 | purine-containing compound metabolic process | 6/41 | 460/18862 | 0.000443896 | 0.015072738 | 0.010144713 | HSD17B4/GAPDH/ADSL/ENO1/FASN/IMPDH2 |
| BP | GO:0033540 | fatty acid beta-oxidation using acyl-CoA oxidase | 2/41 | 15/18862 | 0.000475443 | 0.015134931 | 0.010186572 | HSD17B4/SCP2 |
| BP | GO:0060008 | Sertoli cell differentiation | 2/41 | 15/18862 | 0.000475443 | 0.015134931 | 0.010186572 | HSD17B4/FLNA |
| BP | GO:0071428 | rRNA-containing ribonucleoprotein complex export from nucleus | 2/41 | 15/18862 | 0.000475443 | 0.015134931 | 0.010186572 | ABCE1/NPM1 |
| BP | GO:0032200 | telomere organization | 4/41 | 174/18862 | 0.000542799 | 0.016926464 | 0.011392364 | HNRNPA1/MYC/PTGES3/HNRNPA2B1 |
| BP | GO:0009152 | purine ribonucleotide biosynthetic process | 4/41 | 175/18862 | 0.000554628 | 0.01694942 | 0.011407814 | ADSL/ENO1/FASN/IMPDH2 |
| BP | GO:0032204 | regulation of telomere maintenance | 3/41 | 79/18862 | 0.000672156 | 0.020103097 | 0.013530398 | HNRNPA1/MYC/HNRNPA2B1 |
| BP | GO:0071243 | cellular response to arsenic-containing substance | 2/41 | 18/18862 | 0.000689932 | 0.020103097 | 0.013530398 | HNRNPA1/PPIF |
| BP | GO:0010833 | telomere maintenance via telomere lengthening | 3/41 | 80/18862 | 0.000697293 | 0.020103097 | 0.013530398 | HNRNPA1/PTGES3/HNRNPA2B1 |
| BP | GO:0009260 | ribonucleotide biosynthetic process | 4/41 | 188/18862 | 0.000725593 | 0.020531598 | 0.013818801 | ADSL/ENO1/FASN/IMPDH2 |
| BP | GO:1903311 | regulation of mRNA metabolic process | 5/41 | 334/18862 | 0.000750364 | 0.020642476 | 0.013893427 | HNRNPA1/PSMA3/NPM1/HNRNPA2B1/NUDT21 |
| BP | GO:0050821 | protein stabilization | 4/41 | 191/18862 | 0.000769801 | 0.020642476 | 0.013893427 | GAPDH/PFN1/FLNA/PTGES3 |
| BP | GO:0046485 | ether lipid metabolic process | 2/41 | 19/18862 | 0.00077004 | 0.020642476 | 0.013893427 | FASN/AGPS |
| BP | GO:0006413 | translational initiation | 4/41 | 193/18862 | 0.000800311 | 0.021084066 | 0.014190639 | ABCE1/RPL7A/NPM1/RPS3 |
| BP | GO:0071897 | DNA biosynthetic process | 4/41 | 194/18862 | 0.000815883 | 0.021129996 | 0.014221553 | HNRNPA1/MYC/PTGES3/HNRNPA2B1 |
| BP | GO:0046390 | ribose phosphate biosynthetic process | 4/41 | 195/18862 | 0.000831669 | 0.021179826 | 0.014255091 | ADSL/ENO1/FASN/IMPDH2 |
| BP | GO:0006448 | regulation of translational elongation | 2/41 | 20/18862 | 0.000854423 | 0.021290591 | 0.014329641 | SRP9/EIF5A2 |
| BP | GO:0006164 | purine nucleotide biosynthetic process | 4/41 | 197/18862 | 0.000863885 | 0.021290591 | 0.014329641 | ADSL/ENO1/FASN/IMPDH2 |
| BP | GO:2001233 | regulation of apoptotic signaling pathway | 5/41 | 348/18862 | 0.000902184 | 0.021507482 | 0.01447562 | VDAC2/ENO1/RACK1/RPS3/PPIF |
| BP | GO:0051168 | nuclear export | 4/41 | 201/18862 | 0.000930949 | 0.021507482 | 0.01447562 | HNRNPA1/ABCE1/NPM1/HNRNPA2B1 |
| BP | GO:0002053 | positive regulation of mesenchymal cell proliferation | 2/41 | 21/18862 | 0.000943064 | 0.021507482 | 0.01447562 | MYC/VEGFA |
| BP | GO:0006662 | glycerol ether metabolic process | 2/41 | 21/18862 | 0.000943064 | 0.021507482 | 0.01447562 | FASN/AGPS |
| BP | GO:0009168 | purine ribonucleoside monophosphate biosynthetic process | 2/41 | 21/18862 | 0.000943064 | 0.021507482 | 0.01447562 | ADSL/IMPDH2 |
| BP | GO:0070301 | cellular response to hydrogen peroxide | 3/41 | 90/18862 | 0.000982163 | 0.021948235 | 0.014772269 | RACK1/RPS3/PPIF |
| BP | GO:0043281 | regulation of cysteine-type endopeptidase activity involved in apoptotic process | 4/41 | 205/18862 | 0.001001608 | 0.021948235 | 0.014772269 | MYC/VEGFA/RACK1/RPS3 |
| BP | GO:0017148 | negative regulation of translation | 4/41 | 206/18862 | 0.001019846 | 0.021948235 | 0.014772269 | GAPDH/SRP9/RACK1/RPS3 |
| BP | GO:0071456 | cellular response to hypoxia | 4/41 | 206/18862 | 0.001019846 | 0.021948235 | 0.014772269 | PSMA3/MYC/ENO1/VEGFA |
| BP | GO:0002064 | epithelial cell development | 4/41 | 207/18862 | 0.001038317 | 0.022035401 | 0.014830936 | HSD17B4/FASN/VEGFA/FLNA |
| BP | GO:0072522 | purine-containing compound biosynthetic process | 4/41 | 208/18862 | 0.001057023 | 0.022125087 | 0.014891299 | ADSL/ENO1/FASN/IMPDH2 |
| BP | GO:0009127 | purine nucleoside monophosphate biosynthetic process | 2/41 | 23/18862 | 0.001133045 | 0.023091178 | 0.015541527 | ADSL/IMPDH2 |
| BP | GO:0045862 | positive regulation of proteolysis | 5/41 | 367/18862 | 0.001143567 | 0.023091178 | 0.015541527 | MYC/ENO1/RACK1/SUMO2/RPS3 |
| BP | GO:2001243 | negative regulation of intrinsic apoptotic signaling pathway | 3/41 | 95/18862 | 0.001148514 | 0.023091178 | 0.015541527 | VDAC2/ENO1/PPIF |
| BP | GO:0036294 | cellular response to decreased oxygen levels | 4/41 | 214/18862 | 0.001174273 | 0.02330246 | 0.01568373 | PSMA3/MYC/ENO1/VEGFA |
| BP | GO:0072330 | monocarboxylic acid biosynthetic process | 4/41 | 224/18862 | 0.001389537 | 0.027220665 | 0.01832088 | HSD17B4/FASN/SCP2/PTGES3 |
| BP | GO:0010464 | regulation of mesenchymal cell proliferation | 2/41 | 26/18862 | 0.001449499 | 0.027456713 | 0.018479753 | MYC/VEGFA |
| BP | GO:0018904 | ether metabolic process | 2/41 | 26/18862 | 0.001449499 | 0.027456713 | 0.018479753 | FASN/AGPS |
| BP | GO:0006364 | rRNA processing | 4/41 | 228/18862 | 0.001482893 | 0.027456713 | 0.018479753 | WBP11/NOLC1/RPL7A/PDCD11 |
| BP | GO:2000116 | regulation of cysteine-type endopeptidase activity | 4/41 | 230/18862 | 0.001531177 | 0.027456713 | 0.018479753 | MYC/VEGFA/RACK1/RPS3 |
| BP | GO:0006614 | SRP-dependent cotranslational protein targeting to membrane | 3/41 | 105/18862 | 0.00153226 | 0.027456713 | 0.018479753 | RPL7A/SRP9/RPS3 |
| BP | GO:0071453 | cellular response to oxygen levels | 4/41 | 231/18862 | 0.001555727 | 0.027456713 | 0.018479753 | PSMA3/MYC/ENO1/VEGFA |
| BP | GO:0006735 | NADH regeneration | 2/41 | 27/18862 | 0.001563308 | 0.027456713 | 0.018479753 | GAPDH/ENO1 |
| BP | GO:0061621 | canonical glycolysis | 2/41 | 27/18862 | 0.001563308 | 0.027456713 | 0.018479753 | GAPDH/ENO1 |
| BP | GO:0061718 | glucose catabolic process to pyruvate | 2/41 | 27/18862 | 0.001563308 | 0.027456713 | 0.018479753 | GAPDH/ENO1 |
| BP | GO:2001022 | positive regulation of response to DNA damage stimulus | 3/41 | 107/18862 | 0.001617507 | 0.028002276 | 0.018846944 | MYC/RPS3/H2AX |
| BP | GO:0034249 | negative regulation of cellular amide metabolic process | 4/41 | 234/18862 | 0.001631023 | 0.028002276 | 0.018846944 | GAPDH/SRP9/RACK1/RPS3 |
| BP | GO:0034470 | ncRNA processing | 5/41 | 400/18862 | 0.001672762 | 0.028230201 | 0.019000349 | WBP11/NOLC1/RPL7A/PDCD11/HNRNPA2B1 |
| BP | GO:0061620 | glycolytic process through glucose-6-phosphate | 2/41 | 28/18862 | 0.001681249 | 0.028230201 | 0.019000349 | GAPDH/ENO1 |
| BP | GO:0016072 | rRNA metabolic process | 4/41 | 238/18862 | 0.001735324 | 0.028766877 | 0.019361559 | WBP11/NOLC1/RPL7A/PDCD11 |
| BP | GO:0006613 | cotranslational protein targeting to membrane | 3/41 | 110/18862 | 0.001750864 | 0.028766877 | 0.019361559 | RPL7A/SRP9/RPS3 |
| BP | GO:0061615 | glycolytic process through fructose-6-phosphate | 2/41 | 29/18862 | 0.001803305 | 0.0293133 | 0.019729329 | GAPDH/ENO1 |
| BP | GO:0046685 | response to arsenic-containing substance | 2/41 | 30/18862 | 0.001929459 | 0.030234182 | 0.020349129 | HNRNPA1/PPIF |
| BP | GO:0061099 | negative regulation of protein tyrosine kinase activity | 2/41 | 30/18862 | 0.001929459 | 0.030234182 | 0.020349129 | RACK1/CBLB |
| BP | GO:0090183 | regulation of kidney development | 2/41 | 30/18862 | 0.001929459 | 0.030234182 | 0.020349129 | MYC/VEGFA |
| BP | GO:0051225 | spindle assembly | 3/41 | 114/18862 | 0.001939103 | 0.030234182 | 0.020349129 | SMC3/FLNA/RPS3 |
| BP | GO:0033559 | unsaturated fatty acid metabolic process | 3/41 | 115/18862 | 0.001988055 | 0.030684327 | 0.020652099 | HSD17B4/SCP2/PTGES3 |
| BP | GO:0120254 | olefinic compound metabolic process | 3/41 | 119/18862 | 0.002191559 | 0.033270361 | 0.022392631 | HSD17B4/SCP2/PTGES3 |
| BP | GO:0031334 | positive regulation of protein-containing complex assembly | 4/41 | 254/18862 | 0.002199153 | 0.033270361 | 0.022392631 | PFN1/VEGFA/RACK1/RPS3 |
| BP | GO:0001676 | long-chain fatty acid metabolic process | 3/41 | 120/18862 | 0.002244381 | 0.033295276 | 0.0224094 | HSD17B4/SCP2/PTGES3 |
| BP | GO:0045047 | protein targeting to ER | 3/41 | 120/18862 | 0.002244381 | 0.033295276 | 0.0224094 | RPL7A/SRP9/RPS3 |
| BP | GO:0051973 | positive regulation of telomerase activity | 2/41 | 33/18862 | 0.002332329 | 0.034267291 | 0.023063615 | MYC/PTGES3 |
| BP | GO:0072599 | establishment of protein localization to endoplasmic reticulum | 3/41 | 124/18862 | 0.00246357 | 0.035672993 | 0.024009723 | RPL7A/SRP9/RPS3 |
| BP | GO:0009156 | ribonucleoside monophosphate biosynthetic process | 2/41 | 34/18862 | 0.002474697 | 0.035672993 | 0.024009723 | ADSL/IMPDH2 |
| BP | GO:0045814 | negative regulation of gene expression, epigenetic | 3/41 | 125/18862 | 0.002520363 | 0.035780843 | 0.024082311 | RBBP7/H2AZ1/H2AX |
| BP | GO:0009165 | nucleotide biosynthetic process | 4/41 | 264/18862 | 0.002529012 | 0.035780843 | 0.024082311 | ADSL/ENO1/FASN/IMPDH2 |
| BP | GO:1901293 | nucleoside phosphate biosynthetic process | 4/41 | 267/18862 | 0.002634264 | 0.036928034 | 0.024854429 | ADSL/ENO1/FASN/IMPDH2 |
| BP | GO:0043254 | regulation of protein-containing complex assembly | 5/41 | 446/18862 | 0.002686537 | 0.037318436 | 0.025117189 | VDAC2/PFN1/VEGFA/RACK1/RPS3 |
| BP | GO:0006007 | glucose catabolic process | 2/41 | 36/18862 | 0.002771448 | 0.037810469 | 0.025448352 | GAPDH/ENO1 |
| BP | GO:1904358 | positive regulation of telomere maintenance via telomere lengthening | 2/41 | 36/18862 | 0.002771448 | 0.037810469 | 0.025448352 | HNRNPA1/HNRNPA2B1 |
| BP | GO:0071426 | ribonucleoprotein complex export from nucleus | 3/41 | 130/18862 | 0.002816505 | 0.038085124 | 0.025633209 | ABCE1/NPM1/HNRNPA2B1 |
| BP | GO:0033044 | regulation of chromosome organization | 4/41 | 273/18862 | 0.002853751 | 0.038242445 | 0.025739094 | HNRNPA1/MYC/VEGFA/HNRNPA2B1 |
| BP | GO:0071166 | ribonucleoprotein complex localization | 3/41 | 131/18862 | 0.002878194 | 0.038242445 | 0.025739094 | ABCE1/NPM1/HNRNPA2B1 |
| BP | GO:0030879 | mammary gland development | 3/41 | 132/18862 | 0.002940714 | 0.038736298 | 0.026071482 | NCOR2/FASN/VEGFA |
| BP | GO:0006414 | translational elongation | 3/41 | 134/18862 | 0.003068255 | 0.039567426 | 0.026630873 | SRP9/RACK1/EIF5A2 |

| | | | | | | | | |
|---|---|---|---|---|---|---|---|---|
| BP | GO:0006699 | bile acid biosynthetic process | 2/41 | 38/18862 | 0.003084103 | 0.039567426 | 0.026630873 | HSD17B4/SCP2 |
| BP | GO:0010463 | mesenchymal cell proliferation | 2/41 | 38/18862 | 0.003084103 | 0.039567426 | 0.026630873 | MYC/VEGFA |
| BP | GO:0042542 | response to hydrogen peroxide | 3/41 | 135/18862 | 0.003133284 | 0.039567426 | 0.026630873 | RACK1/RPS3/PPIF |
| BP | GO:0043280 | positive regulation of cysteine-type endopeptidase activity involved in apoptotic process | 3/41 | 135/18862 | 0.003133284 | 0.039567426 | 0.026630873 | MYC/RACK1/RPS3 |
| BP | GO:0071824 | protein-DNA complex subunit organization | 4/41 | 281/18862 | 0.003165525 | 0.039646908 | 0.026684368 | RBBP7/MYC/NPM1/H2AX |
| BP | GO:0060249 | anatomical structure homeostasis | 5/41 | 466/18862 | 0.003243934 | 0.040298623 | 0.027123005 | HNRNPA1/MYC/VEGFA/PTGES3/HNRNPA2B1 |
| BP | GO:0050684 | regulation of mRNA processing | 3/41 | 139/18862 | 0.003401877 | 0.041383625 | 0.027853266 | HNRNPA1/HNRNPA2B1/NUDT21 |
| BP | GO:0009167 | purine ribonucleoside monophosphate metabolic process | 2/41 | 40/18862 | 0.003412524 | 0.041383625 | 0.027853266 | ADSL/IMPDH2 |
| BP | GO:0050856 | regulation of T cell receptor signaling pathway | 2/41 | 40/18862 | 0.003412524 | 0.041383625 | 0.027853266 | RPS3/CBLB |
| BP | GO:0006606 | protein import into nucleus | 3/41 | 143/18862 | 0.003684197 | 0.044326399 | 0.029833902 | NOLC1/FLNA/CBLB |
| BP | GO:0035337 | fatty-acyl-CoA metabolic process | 2/41 | 42/18862 | 0.003756576 | 0.044531826 | 0.029972164 | HSD17B4/FASN |
| BP | GO:0031647 | regulation of protein stability | 4/41 | 295/18862 | 0.00376593 | 0.044531826 | 0.029972164 | GAPDH/PFN1/FLNA/PTGES3 |
| BP | GO:0006334 | nucleosome assembly | 3/41 | 145/18862 | 0.003830573 | 0.044531826 | 0.029972164 | RBBP7/NPM1/H2AX |
| BP | GO:0006734 | NADH metabolic process | 2/41 | 43/18862 | 0.003934422 | 0.044531826 | 0.029972164 | GAPDH/ENO1 |
| BP | GO:0009124 | nucleoside monophosphate biosynthetic process | 2/41 | 43/18862 | 0.003934422 | 0.044531826 | 0.029972164 | ADSL/IMPDH2 |
| BP | GO:0009126 | purine nucleoside monophosphate metabolic process | 2/41 | 43/18862 | 0.003934422 | 0.044531826 | 0.029972164 | ADSL/IMPDH2 |
| BP | GO:0034080 | CENP-A containing nucleosome assembly | 2/41 | 43/18862 | 0.003934422 | 0.044531826 | 0.029972164 | RBBP7/NPM1 |
| BP | GO:0061641 | CENP-A containing chromatin organization | 2/41 | 43/18862 | 0.003934422 | 0.044531826 | 0.029972164 | RBBP7/NPM1 |
| BP | GO:0034660 | ncRNA metabolic process | 5/41 | 492/18862 | 0.004088202 | 0.045932149 | 0.030914652 | WBP11/NOLC1/RPL7A/PDCD11/HNRNPA2B1 |
| BP | GO:2001056 | positive regulation of cysteine-type endopeptidase activity | 3/41 | 151/18862 | 0.004290879 | 0.047857397 | 0.032210441 | MYC/RACK1/RPS3 |
| BP | GO:0051028 | mRNA transport | 3/41 | 152/18862 | 0.004370719 | 0.048046462 | 0.032337692 | HNRNPA1/EIF5A2/HNRNPA2B1 |
| BP | GO:0070972 | protein localization to endoplasmic reticulum | 3/41 | 152/18862 | 0.004370719 | 0.048046462 | 0.032337692 | RPL7A/SRP9/RPS3 |
| BP | GO:0007595 | lactation | 2/41 | 46/18862 | 0.004491034 | 0.049016424 | 0.032990525 | NCOR2/VEGFA |
| BP | GO:0031055 | chromatin remodeling at centromere | 2/41 | 47/18862 | 0.004684207 | 0.050762186 | 0.034165511 | RBBP7/NPM1 |
| BP | GO:0061028 | establishment of endothelial barrier | 2/41 | 48/18862 | 0.004881171 | 0.052524145 | 0.035351398 | FASN/VEGFA |
| BP | GO:0034614 | cellular response to reactive oxygen species | 3/41 | 159/18862 | 0.004954969 | 0.052945404 | 0.035634927 | RACK1/RPS3/PPIF |
| BP | GO:0008206 | bile acid metabolic process | 2/41 | 50/18862 | 0.005286403 | 0.055562882 | 0.037396622 | HSD17B4/SCP2 |
| BP | GO:2000179 | positive regulation of neural precursor cell proliferation | 2/41 | 50/18862 | 0.005286403 | 0.055562882 | 0.037396622 | VEGFA/FLNA |
| BP | GO:0034250 | positive regulation of cellular amide metabolic process | 3/41 | 163/18862 | 0.005309019 | 0.055562882 | 0.037396622 | NPM1/RACK1/EIF5A2 |
| BP | GO:2001252 | positive regulation of chromosome organization | 3/41 | 164/18862 | 0.005399854 | 0.055957088 | 0.037661942 | HNRNPA1/VEGFA/HNRNPA2B1 |
| BP | GO:0046394 | carboxylic acid biosynthetic process | 4/41 | 327/18862 | 0.005419927 | 0.055957088 | 0.037661942 | HSD17B4/FASN/SCP2/PTGES3 |
| BP | GO:0019674 | NAD metabolic process | 2/41 | 51/18862 | 0.005494638 | 0.055972045 | 0.037672009 | GAPDH/ENO1 |
| BP | GO:0032206 | positive regulation of telomere maintenance | 2/41 | 51/18862 | 0.005494638 | 0.055972045 | 0.037672009 | HNRNPA1/HNRNPA2B1 |
| BP | GO:0001658 | branching involved in ureteric bud morphogenesis | 2/41 | 52/18862 | 0.005706598 | 0.057366324 | 0.038610429 | MYC/VEGFA |
| BP | GO:0035196 | production of miRNAs involved in gene silencing by miRNA | 2/41 | 52/18862 | 0.005706598 | 0.057366324 | 0.038610429 | NCOR2/HNRNPA2B1 |
| BP | GO:0016053 | organic acid biosynthetic process | 4/41 | 335/18862 | 0.005898801 | 0.058382074 | 0.03929408 | HSD17B4/FASN/SCP2/PTGES3 |
| BP | GO:0006336 | DNA replication-independent nucleosome assembly | 2/41 | 53/18862 | 0.005922265 | 0.058382074 | 0.03929408 | RBBP7/NPM1 |
| BP | GO:0010332 | response to gamma radiation | 2/41 | 53/18862 | 0.005922265 | 0.058382074 | 0.03929408 | MYC/H2AX |
| BP | GO:0051302 | regulation of cell division | 3/41 | 171/18862 | 0.006062015 | 0.059376659 | 0.039963486 | MYC/VEGFA/RACK1 |
| BP | GO:0034724 | DNA replication-independent nucleosome organization | 2/41 | 54/18862 | 0.006141625 | 0.059773265 | 0.040230421 | RBBP7/NPM1 |
| BP | GO:2000027 | regulation of animal organ morphogenesis | 3/41 | 176/18862 | 0.006563513 | 0.06114225 | 0.041151817 | PFN1/PSMA3/VEGFA |
| BP | GO:0009161 | ribonucleoside monophosphate metabolic process | 2/41 | 56/18862 | 0.006591353 | 0.06114225 | 0.041151817 | ADSL/IMPDH2 |
| BP | GO:0019320 | hexose catabolic process | 2/41 | 56/18862 | 0.006591353 | 0.06114225 | 0.041151817 | GAPDH/ENO1 |
| BP | GO:0031050 | dsRNA processing | 2/41 | 56/18862 | 0.006591353 | 0.06114225 | 0.041151817 | NCOR2/HNRNPA2B1 |
| BP | GO:0034508 | centromere complex assembly | 2/41 | 56/18862 | 0.006591353 | 0.06114225 | 0.041151817 | RBBP7/NPM1 |
| BP | GO:0042306 | regulation of protein import into nucleus | 2/41 | 56/18862 | 0.006591353 | 0.06114225 | 0.041151817 | NOLC1/FLNA |
| BP | GO:0070918 | production of small RNA involved in gene silencing by RNA | 2/41 | 56/18862 | 0.006591353 | 0.06114225 | 0.041151817 | NCOR2/HNRNPA2B1 |
| BP | GO:0010639 | negative regulation of organelle organization | 4/41 | 346/18862 | 0.006602403 | 0.06114225 | 0.041151817 | HNRNPA1/PFN1/NPM1/PPIF |
| BP | GO:0001666 | response to hypoxia | 4/41 | 348/18862 | 0.006736068 | 0.062004291 | 0.041732015 | PSMA3/MYC/ENO1/VEGFA |
| BP | GO:0048008 | platelet-derived growth factor receptor signaling pathway | 2/41 | 57/18862 | 0.006821691 | 0.062416426 | 0.042009402 | VEGFA/CBLB |
| BP | GO:0071103 | DNA conformation change | 4/41 | 352/18862 | 0.007008785 | 0.062718292 | 0.042212573 | RBBP7/NPM1/HNRNPA2B1/H2AX |
| BP | GO:0043486 | histone exchange | 2/41 | 58/18862 | 0.007055654 | 0.062718292 | 0.042212573 | RBBP7/NPM1 |
| BP | GO:0050732 | negative regulation of peptidyl-tyrosine phosphorylation | 2/41 | 58/18862 | 0.007055654 | 0.062718292 | 0.042212573 | RACK1/CBLB |
| BP | GO:0060675 | ureteric bud morphogenesis | 2/41 | 58/18862 | 0.007055654 | 0.062718292 | 0.042212573 | MYC/VEGFA |
| BP | GO:0090150 | establishment of protein localization to membrane | 4/41 | 354/18862 | 0.007147857 | 0.062718292 | 0.042212573 | RPL7A/SRP9/RACK1/RPS3 |
| BP | GO:0007051 | spindle organization | 3/41 | 182/18862 | 0.007197168 | 0.062718292 | 0.042212573 | SMC3/FLNA/RPS3 |
| BP | GO:0010950 | positive regulation of endopeptidase activity | 3/41 | 182/18862 | 0.007197168 | 0.062718292 | 0.042212573 | MYC/RACK1/RPS3 |
| BP | GO:0072171 | mesonephric tubule morphogenesis | 2/41 | 59/18862 | 0.007293229 | 0.062718292 | 0.042212573 | MYC/VEGFA |
| BP | GO:1904589 | regulation of protein import | 2/41 | 59/18862 | 0.007293229 | 0.062718292 | 0.042212573 | NOLC1/FLNA |
| BP | GO:0006611 | protein export from nucleus | 3/41 | 183/18862 | 0.007306188 | 0.062718292 | 0.042212573 | ABCE1/NPM1/HNRNPA2B1 |
| BP | GO:0034728 | nucleosome organization | 3/41 | 183/18862 | 0.007306188 | 0.062718292 | 0.042212573 | RBBP7/NPM1/H2AX |
| BP | GO:0030308 | negative regulation of cell growth | 3/41 | 185/18862 | 0.007527172 | 0.063605313 | 0.042809583 | RBBP7/ENO1/RACK1 |
| BP | GO:1904356 | regulation of telomere maintenance via telomere lengthening | 2/41 | 60/18862 | 0.007534399 | 0.063605313 | 0.042809583 | HNRNPA1/HNRNPA2B1 |
| BP | GO:2001244 | positive regulation of intrinsic apoptotic signaling pathway | 2/41 | 60/18862 | 0.007534399 | 0.063605313 | 0.042809583 | RACK1/RPS3 |
| BP | GO:0036293 | response to decreased oxygen levels | 4/41 | 360/18862 | 0.007576046 | 0.063605486 | 0.0428097 | PSMA3/MYC/ENO1/VEGFA |
| BP | GO:0032233 | positive regulation of actin filament bundle assembly | 2/41 | 62/18862 | 0.008027459 | 0.066302474 | 0.044624908 | PFN1/FLNA |
| BP | GO:0046365 | monosaccharide catabolic process | 2/41 | 62/18862 | 0.008027459 | 0.066302474 | 0.044624908 | GAPDH/ENO1 |
| BP | GO:1902686 | mitochondrial outer membrane permeabilization involved in programmed cell death | 2/41 | 62/18862 | 0.008027459 | 0.066302474 | 0.044624908 | VDAC2/PPIF |
| BP | GO:0006694 | steroid biosynthetic process | 3/41 | 190/18862 | 0.008096898 | 0.066516456 | 0.044768929 | HSD17B4/FASN/SCP2 |
| BP | GO:0071478 | cellular response to radiation | 3/41 | 191/18862 | 0.00821382 | 0.067116135 | 0.045172544 | MYC/NPM1/H2AX |
| BP | GO:0035794 | positive regulation of mitochondrial membrane permeability | 2/41 | 64/18862 | 0.008534708 | 0.069290143 | 0.04663576 | VDAC2/PPIF |
| BP | GO:0017038 | protein import | 3/41 | 194/18862 | 0.008570574 | 0.069290143 | 0.04663576 | NOLC1/FLNA/CBLB |
| BP | GO:0006402 | mRNA catabolic process | 4/41 | 375/18862 | 0.008720042 | 0.070127497 | 0.047199342 | RPL7A/PSMA3/NPM1/RPS3 |
| BP | GO:0090307 | mitotic spindle assembly | 2/41 | 65/18862 | 0.008793613 | 0.070140127 | 0.047207843 | SMC3/FLNA |
| BP | GO:0031497 | chromatin assembly | 3/41 | 196/18862 | 0.008813419 | 0.070140127 | 0.047207843 | RBBP7/NPM1/H2AX |
| BP | GO:0001885 | endothelial cell development | 2/41 | 66/18862 | 0.009056019 | 0.071327819 | 0.048007219 | FASN/VEGFA |
| BP | GO:0050854 | regulation of antigen receptor-mediated signaling pathway | 2/41 | 66/18862 | 0.009056019 | 0.071327819 | 0.048007219 | RPS3/CBLB |
| BP | GO:0010952 | positive regulation of peptidase activity | 3/41 | 200/18862 | 0.009311198 | 0.071618836 | 0.048203088 | MYC/RACK1/RPS3 |
| BP | GO:0009206 | purine ribonucleoside triphosphate biosynthetic process | 2/41 | 67/18862 | 0.009321908 | 0.071618836 | 0.048203088 | ENO1/IMPDH2 |
| BP | GO:0072078 | nephron tubule morphogenesis | 2/41 | 67/18862 | 0.009321908 | 0.071618836 | 0.048203088 | MYC/VEGFA |
| BP | GO:0000377 | RNA splicing, via transesterification reactions with bulged adenosine as nucleophile | 4/41 | 383/18862 | 0.009374193 | 0.071618836 | 0.048203088 | HNRNPA1/WBP11/HNRNPA2B1/NUDT21 |
| BP | GO:0000398 | mRNA splicing, via spliceosome | 4/41 | 383/18862 | 0.009374193 | 0.071618836 | 0.048203088 | HNRNPA1/WBP11/HNRNPA2B1/NUDT21 |
| BP | GO:0042176 | regulation of protein catabolic process | 4/41 | 383/18862 | 0.009374193 | 0.071618836 | 0.048203088 | FLNA/RACK1/SUMO2/CBLB |
| BP | GO:0070482 | response to oxygen levels | 4/41 | 385/18862 | 0.009542613 | 0.072112328 | 0.048535233 | PSMA3/MYC/ENO1/VEGFA |
| BP | GO:0007004 | telomere maintenance via telomerase | 2/41 | 68/18862 | 0.009591266 | 0.072112328 | 0.048535233 | HNRNPA1/PTGES3 |
| BP | GO:0009145 | purine nucleoside triphosphate biosynthetic process | 2/41 | 68/18862 | 0.009591266 | 0.072112328 | 0.048535233 | ENO1/IMPDH2 |
| BP | GO:0000375 | RNA splicing, via transesterification reactions | 4/41 | 386/18862 | 0.009627562 | 0.072112328 | 0.048535233 | HNRNPA1/WBP11/HNRNPA2B1/NUDT21 |
| BP | GO:1902905 | positive regulation of supramolecular fiber organization | 3/41 | 203/18862 | 0.009695165 | 0.072116318 | 0.048537919 | PFN1/FLNA/RPS3 |
| BP | GO:0002573 | myeloid leukocyte differentiation | 3/41 | 204/18862 | 0.009825188 | 0.072116318 | 0.048537919 | MYC/FASN/VEGFA |
| BP | GO:0050852 | T cell receptor signaling pathway | 3/41 | 204/18862 | 0.009825188 | 0.072116318 | 0.048537919 | PSMA3/RPS3/CBLB |
| BP | GO:0072088 | nephron epithelium morphogenesis | 2/41 | 69/18862 | 0.009864078 | 0.072116318 | 0.048537919 | MYC/VEGFA |
| BP | GO:1905710 | positive regulation of membrane permeability | 2/41 | 69/18862 | 0.009864078 | 0.072116318 | 0.048537919 | VDAC2/PPIF |
| BP | GO:0040029 | regulation of gene expression, epigenetic | 3/41 | 205/18862 | 0.009956231 | 0.072443437 | 0.048758086 | RBBP7/H2AZ1/H2AX |
| BP | GO:0006631 | fatty acid metabolic process | 4/41 | 392/18862 | 0.010147667 | 0.073486421 | 0.049460067 | HSD17B4/FASN/SCP2/PTGES3 |
| BP | GO:0061333 | renal tubule morphogenesis | 2/41 | 71/18862 | 0.010419997 | 0.074750022 | 0.050310534 | MYC/VEGFA |
| BP | GO:0072028 | nephron morphogenesis | 2/41 | 71/18862 | 0.010419997 | 0.074750022 | 0.050310534 | MYC/VEGFA |
| BP | GO:0006338 | chromatin remodeling | 3/41 | 209/18862 | 0.010490636 | 0.074905099 | 0.050414909 | RBBP7/MYC/NPM1 |
| BP | GO:0042273 | ribosomal large subunit biogenesis | 2/41 | 72/18862 | 0.010703074 | 0.076066495 | 0.051196587 | RPL7A/NPM1 |
| BP | GO:0006612 | protein targeting to membrane | 3/41 | 211/18862 | 0.010763998 | 0.076145319 | 0.051249639 | RPL7A/SRP9/RPS3 |
| BP | GO:0008406 | gonad development | 3/41 | 212/18862 | 0.010902224 | 0.076767736 | 0.051668558 | HSD17B4/VEGFA/FLNA |
| BP | GO:0009201 | ribonucleoside triphosphate biosynthetic process | 2/41 | 73/18862 | 0.010989542 | 0.077027614 | 0.051843469 | ENO1/IMPDH2 |
| BP | GO:0045739 | positive regulation of DNA repair | 2/41 | 74/18862 | 0.011279386 | 0.078488264 | 0.05282656 | RPS3/H2AX |
| BP | GO:0001558 | regulation of cell growth | 4/41 | 406/18862 | 0.011431732 | 0.078488264 | 0.05282656 | RBBP7/ENO1/VEGFA/RACK1 |
| BP | GO:0042326 | negative regulation of phosphorylation | 4/41 | 407/18862 | 0.011527283 | 0.078488264 | 0.05282656 | NPM1/RACK1/PPIF/CBLB |
| BP | GO:0006278 | RNA-dependent DNA biosynthetic process | 2/41 | 75/18862 | 0.011572591 | 0.078488264 | 0.05282656 | HNRNPA1/PTGES3 |
| BP | GO:0006635 | fatty acid beta-oxidation | 2/41 | 75/18862 | 0.011572591 | 0.078488264 | 0.05282656 | HSD17B4/SCP2 |
| BP | GO:0009123 | nucleoside monophosphate metabolic process | 2/41 | 75/18862 | 0.011572591 | 0.078488264 | 0.05282656 | ADSL/IMPDH2 |
| BP | GO:0046902 | regulation of mitochondrial membrane permeability | 2/41 | 75/18862 | 0.011572591 | 0.078488264 | 0.05282656 | VDAC2/PPIF |
| BP | GO:0045137 | development of primary sexual characteristics | 3/41 | 217/18862 | 0.011608866 | 0.078488264 | 0.05282656 | HSD17B4/VEGFA/FLNA |
| BP | GO:0051495 | positive regulation of cytoskeleton organization | 3/41 | 220/18862 | 0.012045308 | 0.080421951 | 0.054128028 | PFN1/FLNA/RPS3 |
| BP | GO:0006342 | chromatin silencing | 2/41 | 77/18862 | 0.012169021 | 0.080421951 | 0.054128028 | H2AZ1/H2AX |
| BP | GO:0061418 | regulation of transcription from RNA polymerase II promoter in response to hypoxia | 2/41 | 77/18862 | 0.012169021 | 0.080421951 | 0.054128028 | PSMA3/VEGFA |
| BP | GO:0006333 | chromatin assembly or disassembly | 3/41 | 221/18862 | 0.012192873 | 0.080421951 | 0.054128028 | RBBP7/NPM1/H2AX |
| BP | GO:2001020 | regulation of response to DNA damage stimulus | 3/41 | 221/18862 | 0.012192873 | 0.080421951 | 0.054128028 | MYC/RPS3/H2AX |
| BP | GO:0006401 | RNA catabolic process | 4/41 | 414/18862 | 0.012210663 | 0.080421951 | 0.054128028 | RPL7A/PSMA3/NPM1/RPS3 |
| BP | GO:0032272 | negative regulation of protein polymerization | 2/41 | 78/18862 | 0.012472216 | 0.081792042 | 0.055050169 | VDAC2/PFN1 |
| BP | GO:0000302 | response to reactive oxygen species | 3/41 | 224/18862 | 0.012641836 | 0.082198832 | 0.055323959 | RACK1/RPS3/PPIF |
| BP | GO:2001234 | negative regulation of apoptotic signaling pathway | 3/41 | 224/18862 | 0.012641836 | 0.082198832 | 0.055323959 | VDAC2/ENO1/PPIF |
| BP | GO:0032271 | regulation of protein polymerization | 3/41 | 225/18862 | 0.012793584 | 0.082483529 | 0.055515575 | VDAC2/PFN1/RPS3 |

| | | | | | | | | |
|---|---|---|---|---|---|---|---|---|
| BP | GO:0045732 | positive regulation of protein catabolic process | 3/41 | 225/18862 | 0.012793584 | 0.082483529 | 0.055515575 | RACK1/SUMO2/CBLB |
| BP | GO:0009205 | purine ribonucleoside triphosphate metabolic process | 2/41 | 80/18862 | 0.013088491 | 0.084030311 | 0.056556637 | ENO1/IMPDH2 |
| BP | GO:0043161 | proteasome-mediated ubiquitin-dependent protein catabolic process | 4/41 | 425/18862 | 0.01333651 | 0.08526438 | 0.057387227 | PSMA3/RACK1/SUMO2/ARMC8 |
| BP | GO:0043462 | regulation of ATPase activity | 2/41 | 81/18862 | 0.013401541 | 0.085323142 | 0.057426777 | PFN1/PPIF |
| BP | GO:1901568 | fatty acid derivative metabolic process | 2/41 | 82/18862 | 0.013717845 | 0.086615156 | 0.058296368 | HSD17B4/FASN |
| BP | GO:2000177 | regulation of neural precursor cell proliferation | 2/41 | 82/18862 | 0.013717845 | 0.086615156 | 0.058296368 | VEGFA/FLNA |
| BP | GO:0044282 | small molecule catabolic process | 4/41 | 431/18862 | 0.013977773 | 0.087893155 | 0.059156525 | HSD17B4/GAPDH/ENO1/SCP2 |
| BP | GO:0009142 | nucleoside triphosphate biosynthetic process | 2/41 | 84/18862 | 0.01436016 | 0.08992756 | 0.060525783 | ENO1/IMPDH2 |
| BP | GO:0062012 | regulation of small molecule metabolic process | 4/41 | 437/18862 | 0.014638467 | 0.091296237 | 0.061446971 | NCOR2/PSMA3/ENO1/FASN |
| BP | GO:0001657 | ureteric bud development | 2/41 | 86/18862 | 0.015015316 | 0.092299431 | 0.062122172 | MYC/VEGFA |
| BP | GO:0007589 | body fluid secretion | 2/41 | 86/18862 | 0.015015316 | 0.092299431 | 0.062122172 | NCOR2/VEGFA |
| BP | GO:0009144 | purine nucleoside triphosphate metabolic process | 2/41 | 86/18862 | 0.015015316 | 0.092299431 | 0.062122172 | ENO1/IMPDH2 |
| BP | GO:0006323 | DNA packaging | 3/41 | 240/18862 | 0.015196251 | 0.092299431 | 0.062122172 | RBBP7/NPM1/H2AX |
| BP | GO:0009199 | ribonucleoside triphosphate metabolic process | 2/41 | 87/18862 | 0.015347673 | 0.092299431 | 0.062122172 | ENO1/IMPDH2 |
| BP | GO:0072163 | mesonephric epithelium development | 2/41 | 87/18862 | 0.015347673 | 0.092299431 | 0.062122172 | MYC/VEGFA |
| BP | GO:0072164 | mesonephric tubule development | 2/41 | 87/18862 | 0.015347673 | 0.092299431 | 0.062122172 | MYC/VEGFA |
| BP | GO:0065004 | protein-DNA complex assembly | 3/41 | 241/18862 | 0.015364903 | 0.092299431 | 0.062122172 | RBBP7/NPM1/H2AX |
| BP | GO:0051090 | regulation of DNA-binding transcription factor activity | 4/41 | 444/18862 | 0.015434095 | 0.092299431 | 0.062122172 | NPM1/VEGFA/FLNA/RPS3 |
| BP | GO:0006094 | gluconeogenesis | 2/41 | 88/18862 | 0.015683196 | 0.092299431 | 0.062122172 | GAPDH/ENO1 |
| BP | GO:0032436 | positive regulation of proteasomal ubiquitin-dependent protein catabolic process | 2/41 | 88/18862 | 0.015683196 | 0.092299431 | 0.062122172 | RACK1/SUMO2 |
| BP | GO:0034644 | cellular response to UV | 2/41 | 88/18862 | 0.015683196 | 0.092299431 | 0.062122172 | MYC/NPM1 |
| BP | GO:0060993 | kidney morphogenesis | 2/41 | 88/18862 | 0.015683196 | 0.092299431 | 0.062122172 | MYC/VEGFA |
| BP | GO:0072080 | nephron tubule development | 2/41 | 88/18862 | 0.015683196 | 0.092299431 | 0.062122172 | MYC/VEGFA |
| BP | GO:0006469 | negative regulation of protein kinase activity | 3/41 | 243/18862 | 0.015705401 | 0.092299431 | 0.062122172 | NPM1/RACK1/CBLB |
| BP | GO:0043044 | ATP-dependent chromatin remodeling | 2/41 | 89/18862 | 0.016021871 | 0.093249606 | 0.062761687 | RBBP7/NPM1 |
| BP | GO:1901532 | regulation of hematopoietic progenitor cell differentiation | 2/41 | 89/18862 | 0.016021871 | 0.093249606 | 0.062761687 | PSMA3/NUDT21 |
| BP | GO:0045926 | negative regulation of growth | 3/41 | 245/18862 | 0.016050161 | 0.093249606 | 0.062761687 | RBBP7/ENO1/RACK1 |
| BP | GO:0061326 | renal tubule development | 2/41 | 90/18862 | 0.016363682 | 0.094353609 | 0.063504737 | MYC/VEGFA |
| BP | GO:0090559 | regulation of membrane permeability | 2/41 | 90/18862 | 0.016363682 | 0.094353609 | 0.063504737 | VDAC2/PPIF |
| BP | GO:0001823 | mesonephros development | 2/41 | 91/18862 | 0.016708616 | 0.095620844 | 0.06435765 | MYC/VEGFA |
| BP | GO:0019319 | hexose biosynthetic process | 2/41 | 91/18862 | 0.016708616 | 0.095620844 | 0.06435765 | GAPDH/ENO1 |
| BP | GO:0051346 | negative regulation of hydrolase activity | 4/41 | 456/18862 | 0.016861018 | 0.09613297 | 0.064702337 | GAPDH/ABCE1/VEGFA/PPIF |
| BP | GO:0048863 | stem cell differentiation | 3/41 | 251/18862 | 0.017110081 | 0.096830382 | 0.06517173 | NOLC1/PSMA3/NUDT21 |
| BP | GO:1901617 | organic hydroxy compound biosynthetic process | 3/41 | 251/18862 | 0.017110081 | 0.096830382 | 0.06517173 | HSD17B4/FASN/SCP2 |
| BP | GO:0006476 | protein deacetylation | 2/41 | 94/18862 | 0.017762008 | 0.099780694 | 0.067157438 | VEGFA/FLNA |
| BP | GO:0061097 | regulation of protein tyrosine kinase activity | 2/41 | 94/18862 | 0.017762008 | 0.099780694 | 0.067157438 | RACK1/CBLB |
| CC | GO:0005782 | peroxisomal matrix | 4/41 | 51/19520 | 3.90E-06 | 0.000315639 | 0.000213297 | HSD17B4/SCP2/AGPS/GSTK1 |
| CC | GO:0031907 | microbody lumen | 4/41 | 51/19520 | 3.90E-06 | 0.000315639 | 0.000213297 | HSD17B4/SCP2/AGPS/GSTK1 |
| CC | GO:0005777 | peroxisome | 5/41 | 136/19520 | 9.34E-06 | 0.000378331 | 0.000255663 | HSD17B4/IMPDH2/SCP2/AGPS/GSTK1 |
| CC | GO:0042579 | microbody | 5/41 | 136/19520 | 9.34E-06 | 0.000378331 | 0.000255663 | HSD17B4/IMPDH2/SCP2/AGPS/GSTK1 |
| CC | GO:0005778 | peroxisomal membrane | 3/41 | 61/19520 | 0.000284425 | 0.007679484 | 0.005189515 | HSD17B4/IMPDH2/AGPS |
| CC | GO:0031903 | microbody membrane | 3/41 | 61/19520 | 0.000284425 | 0.007679484 | 0.005189515 | HSD17B4/IMPDH2/AGPS |
| CC | GO:0046930 | pore complex | 2/41 | 23/19520 | 0.001058975 | 0.024507697 | 0.016561407 | VDAC2/PPIF |
| CC | GO:0016363 | nuclear matrix | 3/41 | 109/19520 | 0.001547218 | 0.02980835 | 0.020143394 | SMC3/NCOR2/HNRNPA2B1 |
| CC | GO:0005925 | focal adhesion | 5/41 | 416/19520 | 0.001710339 | 0.02980835 | 0.020143394 | PFN1/RPL7A/NPM1/FLNA/RPS3 |
| CC | GO:0030055 | cell-substrate junction | 5/41 | 423/19520 | 0.001840022 | 0.02980835 | 0.020143394 | PFN1/RPL7A/NPM1/FLNA/RPS3 |
| CC | GO:0034399 | nuclear periphery | 3/41 | 128/19520 | 0.002447517 | 0.036045247 | 0.024358062 | SMC3/NCOR2/HNRNPA2B1 |
| CC | GO:0005759 | mitochondrial matrix | 5/41 | 476/19520 | 0.003068817 | 0.041429027 | 0.027996224 | VDAC2/ABCE1/RPS3/GSTK1/PPIF |
| CC | GO:0000781 | chromosome, telomeric region | 3/41 | 161/19520 | 0.004665715 | 0.058141985 | 0.039290231 | PTGES3/HNRNPA2B1/H2AX |
| CC | GO:0098687 | chromosomal region | 4/41 | 345/19520 | 0.005801403 | 0.067130524 | 0.045364357 | SMC3/PTGES3/HNRNPA2B1/H2AX |
| CC | GO:0044391 | ribosomal subunit | 3/41 | 187/19520 | 0.00705946 | 0.075749395 | 0.051188675 | RPL7A/RACK1/RPS3 |
| CC | GO:0005681 | spliceosomal complex | 3/41 | 191/19520 | 0.007481422 | 0.075749395 | 0.051188675 | HNRNPA1/WBP11/HNRNPA2B1 |
| CC | GO:0005844 | polysome | 2/41 | 68/19520 | 0.008982835 | 0.084960975 | 0.057413525 | RPL7A/RPS3 |
| CC | GO:0032993 | protein-DNA complex | 3/41 | 208/19520 | 0.009440108 | 0.084960975 | 0.057413525 | H2AZ1/NPM1/H2AX |
| CC | GO:0015935 | small ribosomal subunit | 2/41 | 74/19520 | 0.010566763 | 0.085590781 | 0.057839124 | RACK1/RPS3 |
| CC | GO:0017053 | transcription repressor complex | 2/41 | 74/19520 | 0.010566763 | 0.085590781 | 0.057839124 | RBBP7/NCOR2 |
| CC | GO:0000118 | histone deacetylase complex | 2/41 | 77/19520 | 0.011401752 | 0.086054128 | 0.058152237 | RBBP7/NCOR2 |
| CC | GO:0015030 | Cajal body | 2/41 | 78/19520 | 0.011686363 | 0.086054128 | 0.058152237 | NOLC1/HNRNPA2B1 |
| CC | GO:0005840 | ribosome | 3/41 | 243/19520 | 0.014341939 | 0.095267122 | 0.064378042 | RPL7A/RACK1/RPS3 |
| CC | GO:0071013 | catalytic step 2 spliceosome | 2/41 | 87/19520 | 0.014386537 | 0.095267122 | 0.064378042 | HNRNPA1/HNRNPA2B1 |
| CC | GO:0000794 | condensed nuclear chromosome | 2/41 | 88/19520 | 0.014701716 | 0.095267122 | 0.064378042 | SMC3/H2AX |
| MF | GO:0043021 | ribonucleoprotein complex binding | 6/41 | 134/18337 | 4.96E-07 | 0.000118042 | 8.46E-05 | NOLC1/ABCE1/NPM1/SRP9/RACK1/EIF5A2 |
| MF | GO:0016835 | carbon-oxygen lyase activity | 4/41 | 79/18337 | 2.86E-05 | 0.003406392 | 0.00244067 | HSD17B4/ENO1/FASN/RPS3 |
| MF | GO:0016829 | lyase activity | 5/41 | 194/18337 | 6.92E-05 | 0.004606675 | 0.003300669 | HSD17B4/ADSL/ENO1/FASN/RPS3 |
| MF | GO:0045296 | cadherin binding | 6/41 | 332/18337 | 8.87E-05 | 0.004606675 | 0.003300669 | PFN1/RPL7A/ENO1/FASN/FLNA/RACK1 |
| MF | GO:0001046 | core promoter sequence-specific DNA binding | 3/41 | 40/18337 | 9.68E-05 | 0.004606675 | 0.003300669 | H2AZ1/MYC/NPM1 |
| MF | GO:0098505 | G-rich strand telomeric DNA binding | 2/41 | 10/18337 | 0.000217018 | 0.008608376 | 0.006167877 | HNRNPA1/HNRNPA2B1 |
| MF | GO:0043047 | single-stranded telomeric DNA binding | 2/41 | 12/18337 | 0.000317392 | 0.010791324 | 0.007731952 | HNRNPA1/HNRNPA2B1 |
| MF | GO:0016836 | hydro-lyase activity | 3/41 | 64/18337 | 0.000393204 | 0.011697819 | 0.008381453 | HSD17B4/ENO1/FASN |
| MF | GO:0098847 | sequence-specific single stranded DNA binding | 2/41 | 15/18337 | 0.0005028 | 0.013296261 | 0.009526733 | HNRNPA1/HNRNPA2B1 |
| MF | GO:0043024 | ribosomal small subunit binding | 2/41 | 17/18337 | 0.000649403 | 0.015455795 | 0.011074033 | ABCE1/NPM1 |
| MF | GO:0033218 | amide binding | 5/41 | 391/18337 | 0.00171256 | 0.03705357 | 0.026548776 | NOLC1/VDAC2/FASN/SCP2/PPIF |
| MF | GO:0003697 | single-stranded DNA binding | 3/41 | 116/18337 | 0.00220711 | 0.041901371 | 0.030022212 | HNRNPA1/WBP11/HNRNPA2B1 |
| MF | GO:0016616 | oxidoreductase activity, acting on the CH-OH group of donors, NAD or NADP as acceptor | 3/41 | 120/18337 | 0.002430472 | 0.041901371 | 0.030022212 | HSD17B4/FASN/IMPDH2 |
| MF | GO:0035198 | miRNA binding | 2/41 | 33/18337 | 0.002464787 | 0.041901371 | 0.030022212 | HNRNPA1/HNRNPA2B1 |
| MF | GO:0042162 | telomeric DNA binding | 2/41 | 36/18337 | 0.0029285 | 0.04534989 | 0.032493066 | HNRNPA1/HNRNPA2B1 |
| MF | GO:0016614 | oxidoreductase activity, acting on CH-OH group of donors | 3/41 | 130/18337 | 0.003048732 | 0.04534989 | 0.032493066 | HSD17B4/FASN/IMPDH2 |
| MF | GO:0044390 | ubiquitin-like protein conjugating enzyme binding | 2/41 | 39/18337 | 0.003429912 | 0.048018767 | 0.034405308 | ZMYM2/RPS3 |
| MF | GO:0051879 | Hsp90 protein binding | 2/41 | 41/18337 | 0.003784883 | 0.050044559 | 0.035856783 | RPS3/PTGES3 |
| MF | GO:0001784 | phosphotyrosine residue binding | 2/41 | 44/18337 | 0.004348015 | 0.054071619 | 0.03874216 | PFN1/CBLB |
| MF | GO:0061980 | regulatory RNA binding | 2/41 | 45/18337 | 0.004543834 | 0.054071619 | 0.03874216 | HNRNPA1/HNRNPA2B1 |
| MF | GO:0016853 | isomerase activity | 3/41 | 157/18337 | 0.005171944 | 0.058615366 | 0.041997741 | HSD17B4/PPIF/PTGES3 |
| MF | GO:0015485 | cholesterol binding | 2/41 | 50/18337 | 0.005582916 | 0.059927476 | 0.042937864 | VDAC2/SCP2 |
| MF | GO:0046982 | protein heterodimerization activity | 4/41 | 324/18337 | 0.005791311 | 0.059927476 | 0.042937864 | SMC3/NOLC1/H2AZ1/H2AX |
| MF | GO:0005080 | protein kinase C binding | 2/41 | 54/18337 | 0.006485096 | 0.063487403 | 0.045488542 | FLNA/RACK1 |
| MF | GO:0045309 | protein phosphorylated amino acid binding | 2/41 | 56/18337 | 0.006959433 | 0.063487403 | 0.045488542 | PFN1/CBLB |
| MF | GO:0016765 | transferase activity, transferring alkyl or aryl (other than methyl) groups | 2/41 | 57/18337 | 0.007202352 | 0.063487403 | 0.045488542 | AGPS/GSTK1 |
| MF | GO:0043022 | ribosome binding | 2/41 | 57/18337 | 0.007202352 | 0.063487403 | 0.045488542 | RACK1/EIF5A2 |
| MF | GO:0036002 | pre-mRNA binding | 2/41 | 59/18337 | 0.007699605 | 0.065276856 | 0.04677068 | HNRNPA1/HNRNPA2B1 |
| MF | GO:0032934 | sterol binding | 2/41 | 60/18337 | 0.007953903 | 0.065276856 | 0.04677068 | VDAC2/SCP2 |
| MF | GO:0003684 | damaged DNA binding | 2/41 | 66/18337 | 0.009558015 | 0.075826916 | 0.054329767 | RPS3/H2AX |
| MF | GO:0004860 | protein kinase inhibitor activity | 2/41 | 69/18337 | 0.010409654 | 0.078120939 | 0.055973428 | NPM1/RACK1 |
| MF | GO:0004857 | enzyme inhibitor activity | 4/41 | 385/18337 | 0.010503656 | 0.078120939 | 0.055973428 | GAPDH/ABCE1/NPM1/RACK1 |
| MF | GO:0030971 | receptor tyrosine kinase binding | 2/41 | 72/18337 | 0.01129374 | 0.081168976 | 0.058157338 | RACK1/CBLB |
| MF | GO:0019210 | kinase inhibitor activity | 2/41 | 73/18337 | 0.011595568 | 0.081168976 | 0.058157338 | NPM1/RACK1 |
| MF | GO:0033613 | activating transcription factor binding | 2/41 | 78/18337 | 0.013157457 | 0.089470709 | 0.064105506 | MYC/NPM1 |